

**Electronic Supplementary Information
(ESI)**

A rare isostructural series of 3d-4f cyanido-bridged heterobimetallic squares obtained by assembling $[Fe\{HB(pz)_3\}(CN)_3]^-$ and lanthanide ions: synthesis, X-ray structures and cryomagnetic istudy

Maria-Gabriela Alexandru,^a Diana Visinescu,*^b Beatrice Braun-Cula,^c Sergiu Shova,^d Renato Rabelo,^c Nicolás Moliner,^c Francesc Lloret,^e Joan Cano*^e and Miguel Julve*^e

^a*Department of Inorganic Chemistry, Physical Chemistry and Electrochemistry, Faculty of Applied Chemistry and Materials Science, University Politehnica of Bucharest, 1-7 Gh. Polizu Street, 011061 Bucharest, Romania*

^b*Coordination and Supramolecular Chemistry Laboratory, “Ilie Murgulescu” Institute of Physical Chemistry, Romanian Academy, Splaiul Independentei 202, Bucharest 060021, Romania. E-mail: diana.visinescu@gmail.com*

^c*Department of Chemistry, Humboldt-Universität zu Berlin, Brook-Taylor-Str. 2, 12489 Berlin, Germany*

^d*Petru Poni” Institute of Macromolecular Chemistry, Romanian Academy, Aleea Grigore Ghica Vodă 41-A, RO-700487 Iasi, Romania*

^e*Departament de Química Inorgànica/Instituto de Ciencia Molecular, Universitat de València, C/Catedrático José Beltrán 2, 46980 Paterna, València, Spain. E-mail: miguel.julve@uv.es; joan.cano@uv.es*

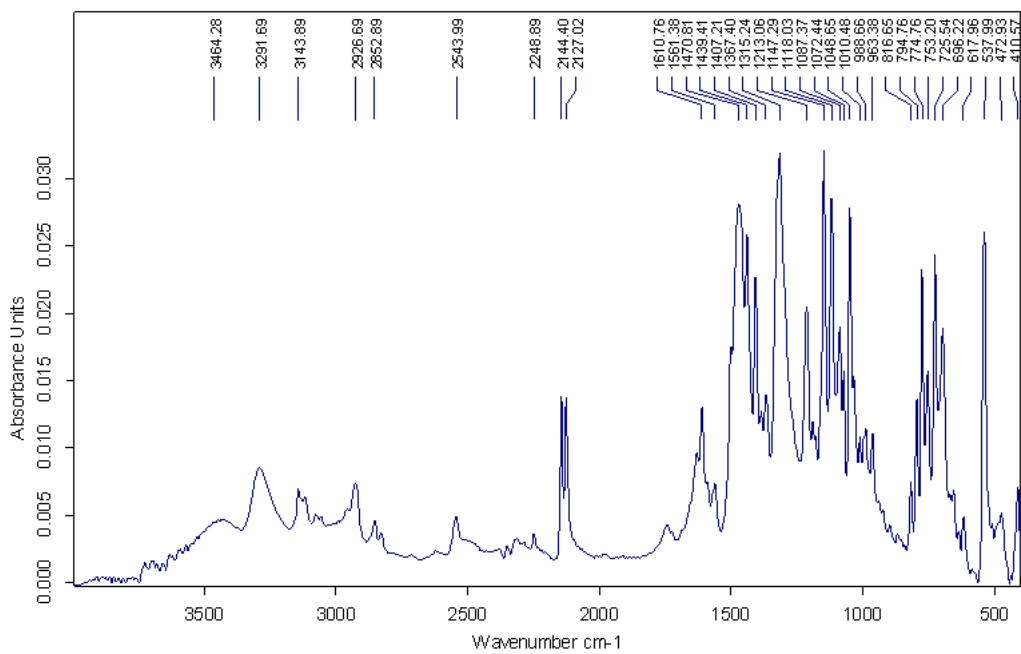


Fig. S1. FTIR spectrum of **1**.

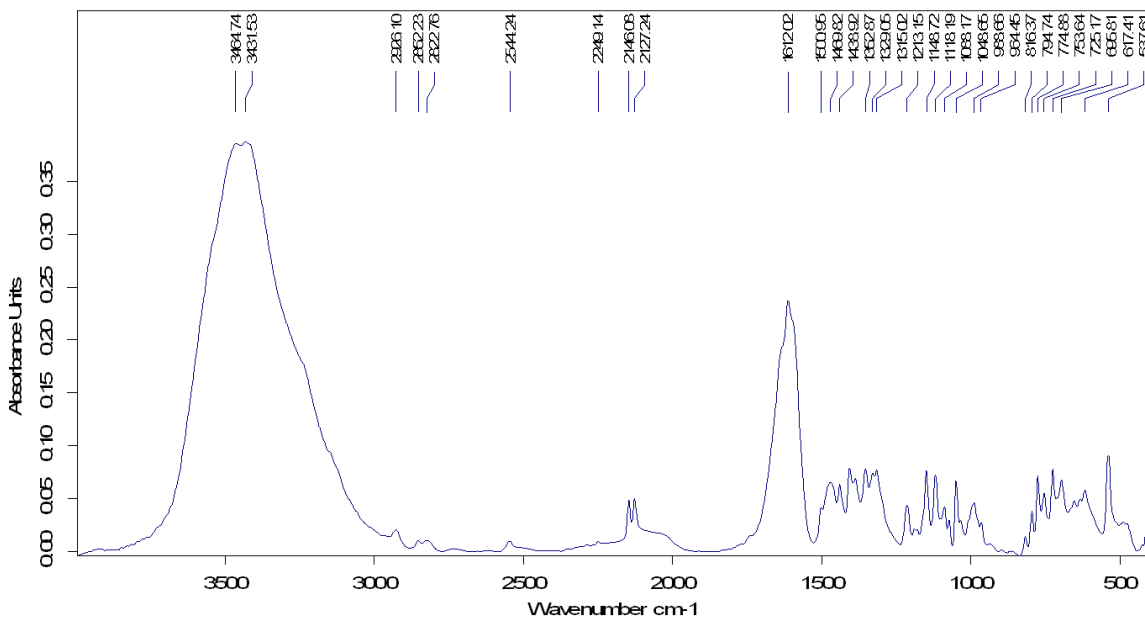


Fig. S2. FTIR spectrum of **2**.

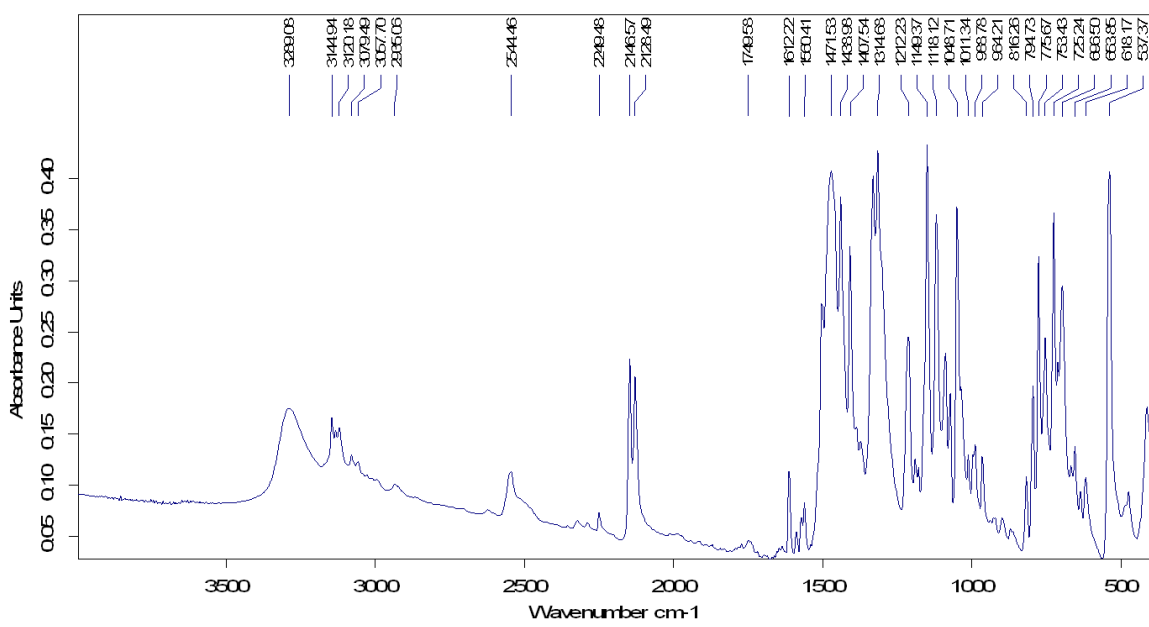


Fig. S3. FTIR spectrum of **3**.

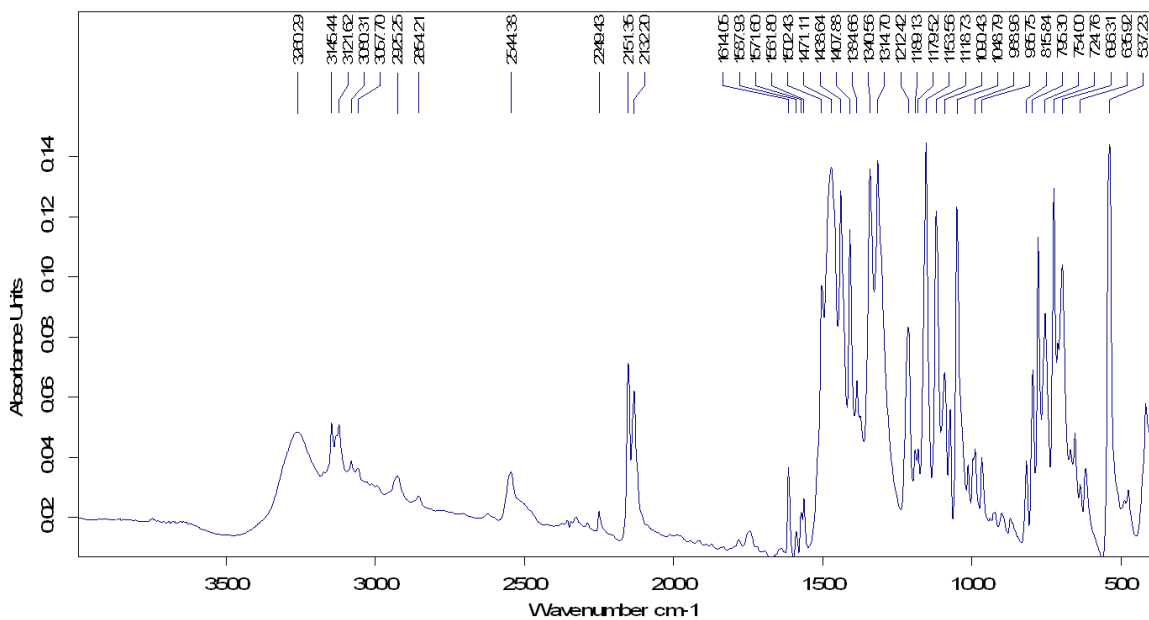


Fig. S4. FTIR spectrum of **4**.

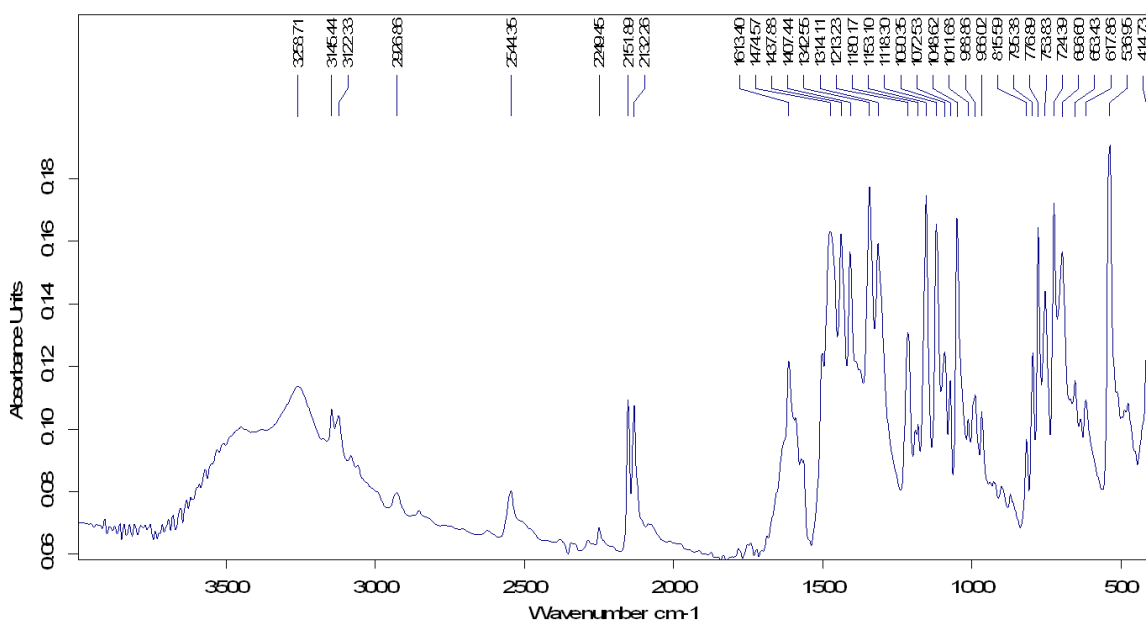


Fig. S5. FTIR spectrum of **5**.

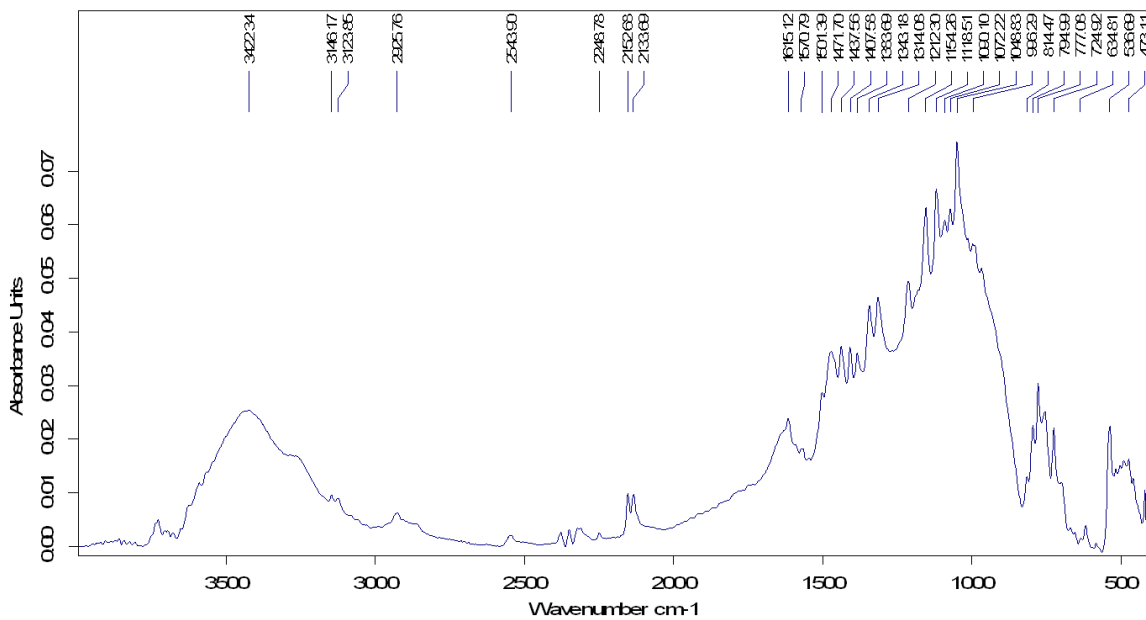


Fig. S6. FTIR spectrum of **6**.

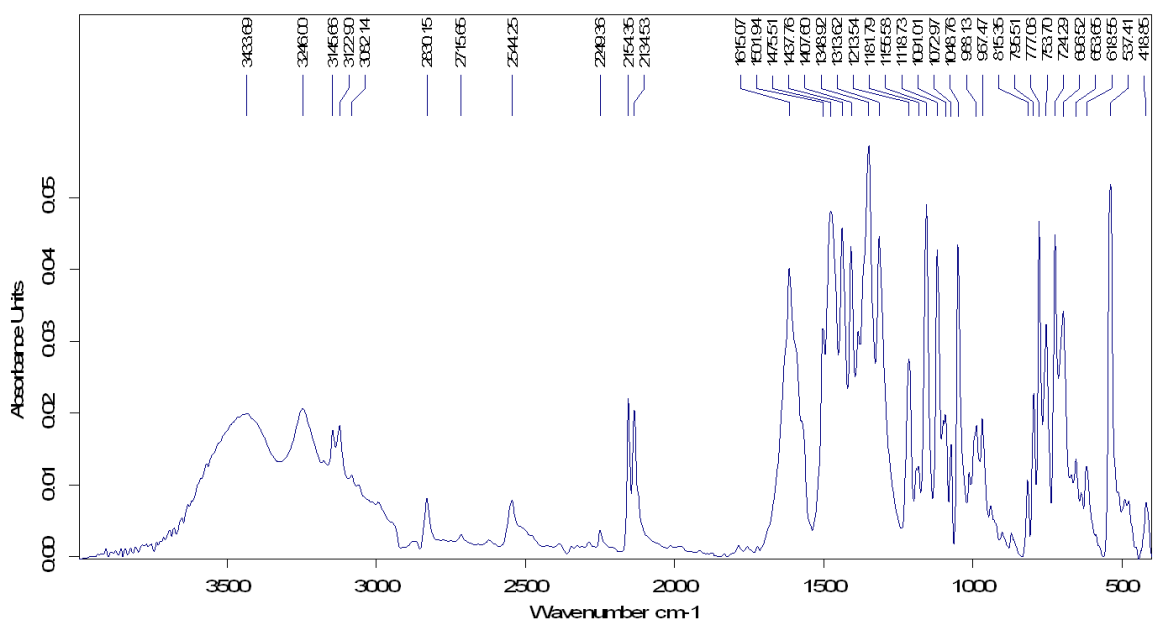


Fig. S7. FTIR spectrum of **7**.

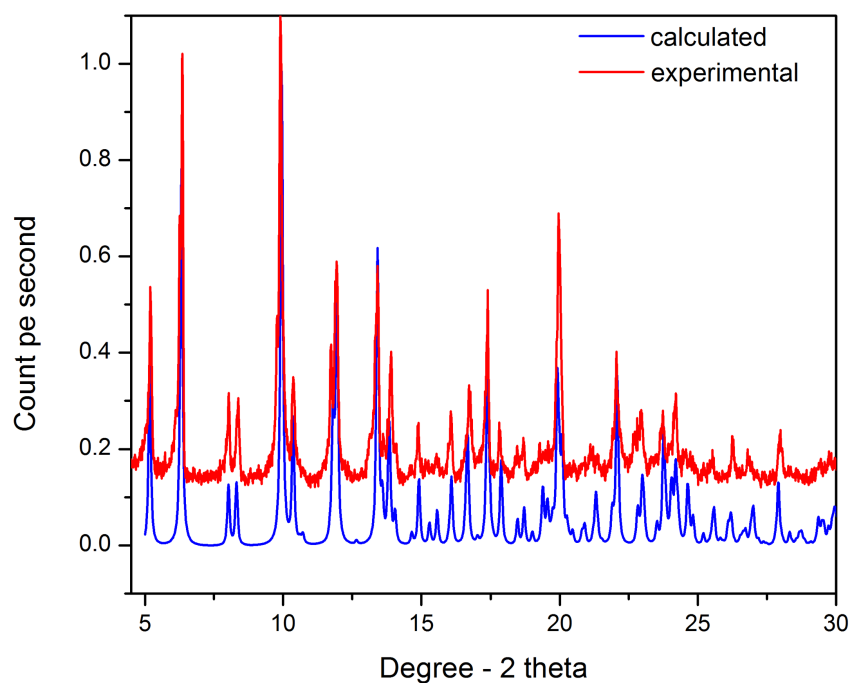


Fig. S8. Experimental and calculated powder X-ray diffractograms at room temperature for 1.

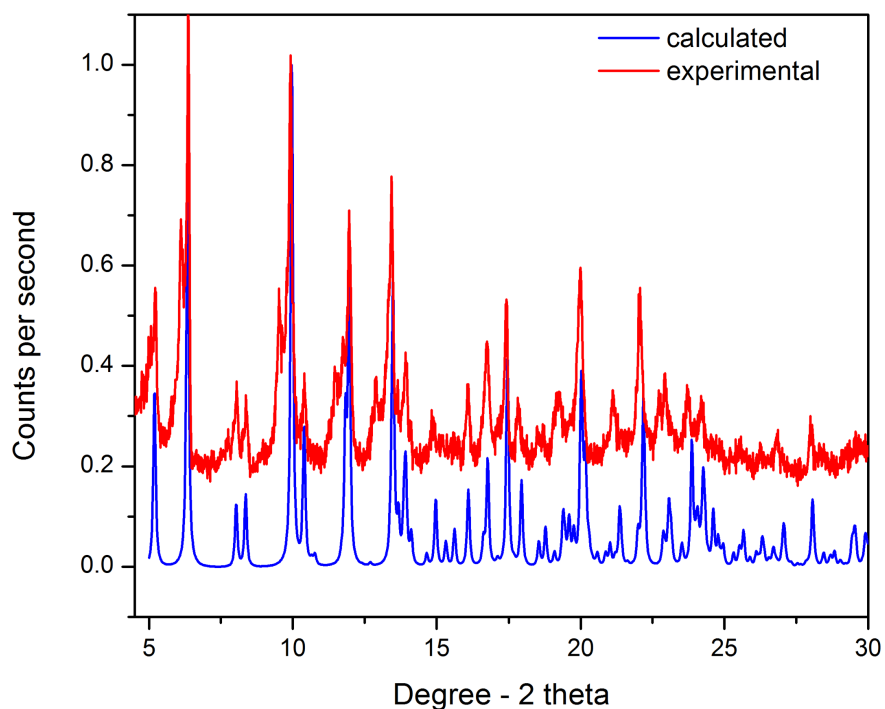


Fig. S9. Experimental and calculated powder X-ray diffractograms at room temperature for 2.

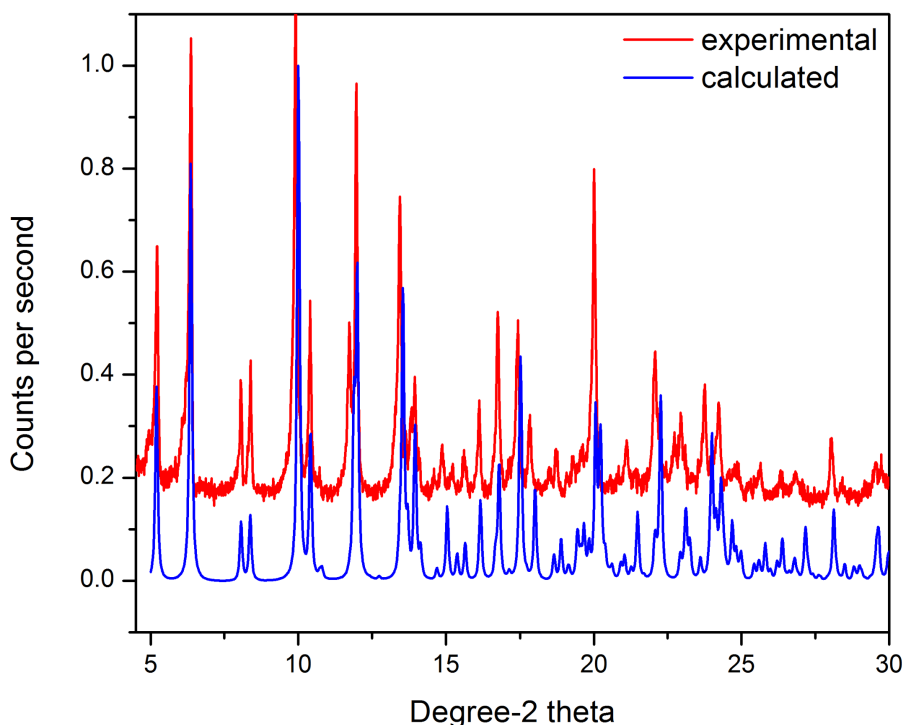


Fig. S10. Experimental and calculated powder X-ray diffractograms at room temperature for 3.

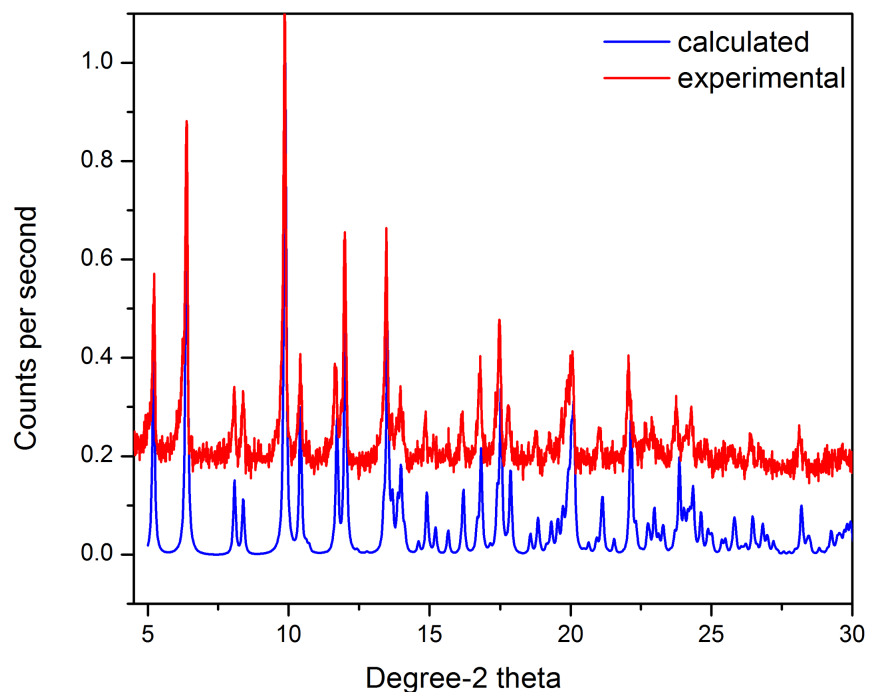


Fig. S11. Experimental and calculated powder X-ray diffractograms at room temperature for 4.

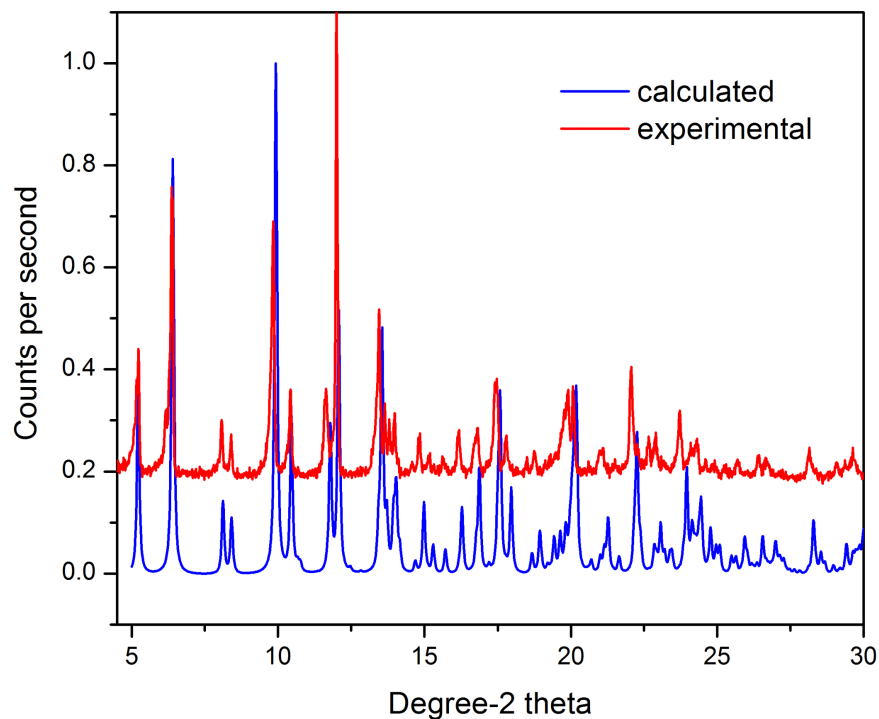


Fig. S12. Experimental and calculated powder X-ray diffractograms at room temperature for 5.

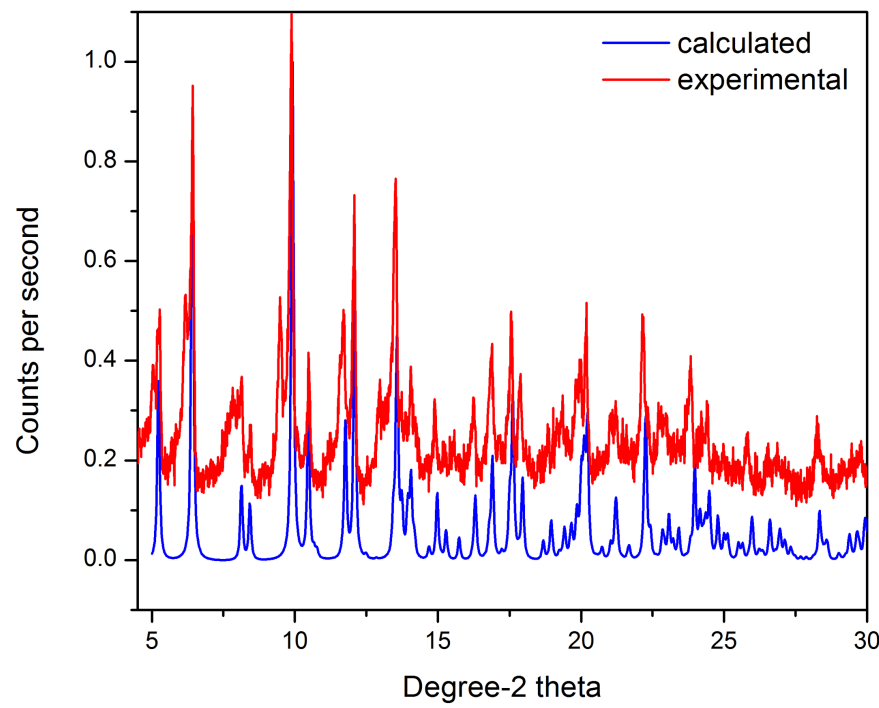


Fig. S13. Experimental and calculated powder X-ray diffractograms at room temperature for 6.

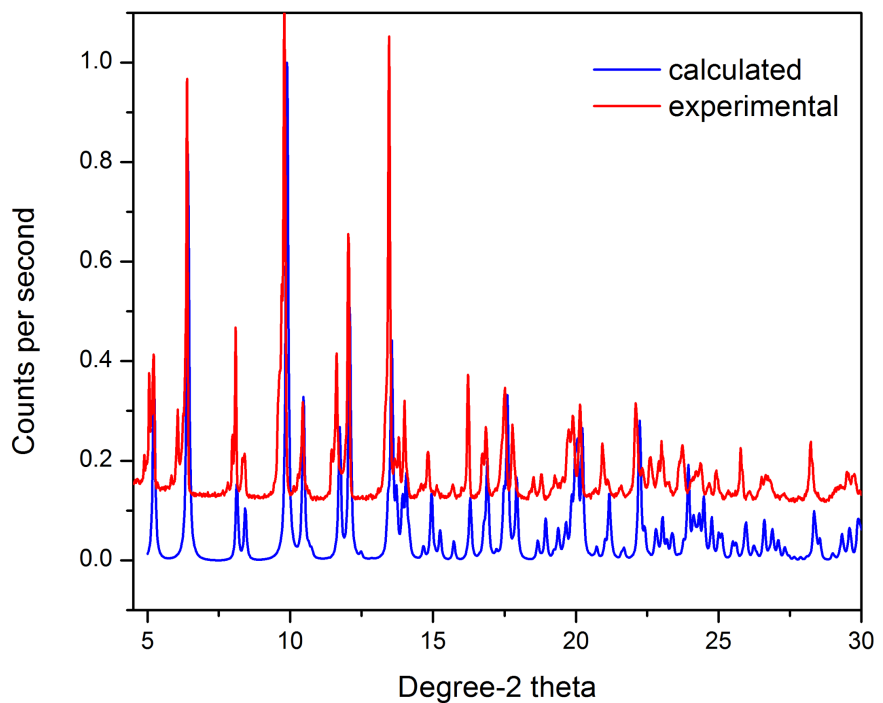


Fig. S14. Experimental and calculated powder X-ray diffractograms at room temperature for 7.

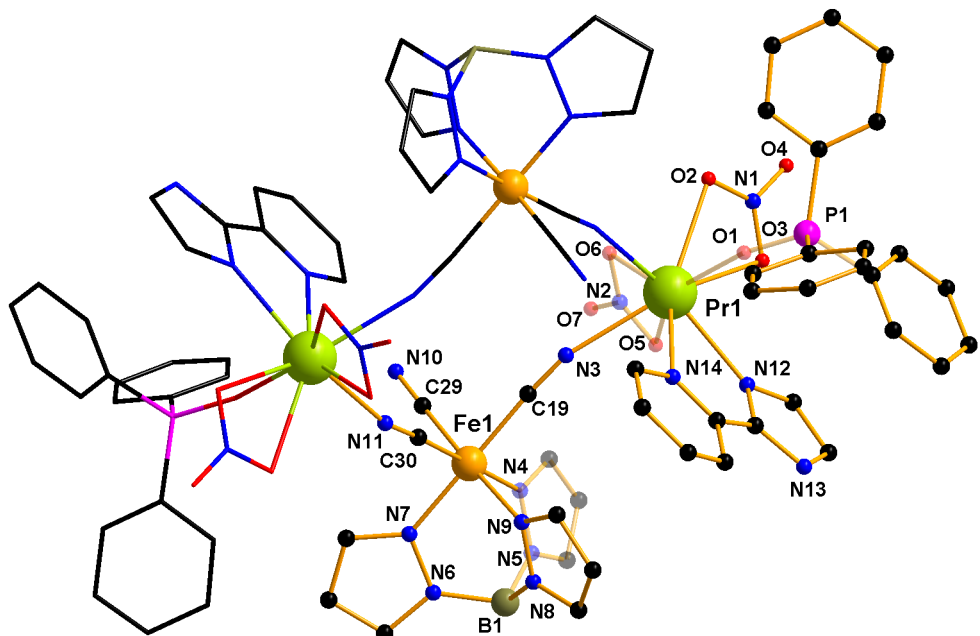


Fig. S15. View of the square-shaped cyanido-bridged heterometallic unit in **2** together with the atom labelling scheme (the molecular fragment generated by the inversion symmetry operation is represented as wires and sticks) [symmetry code (*a*) = 1-*x*, 1-*y*, 1-*z*].

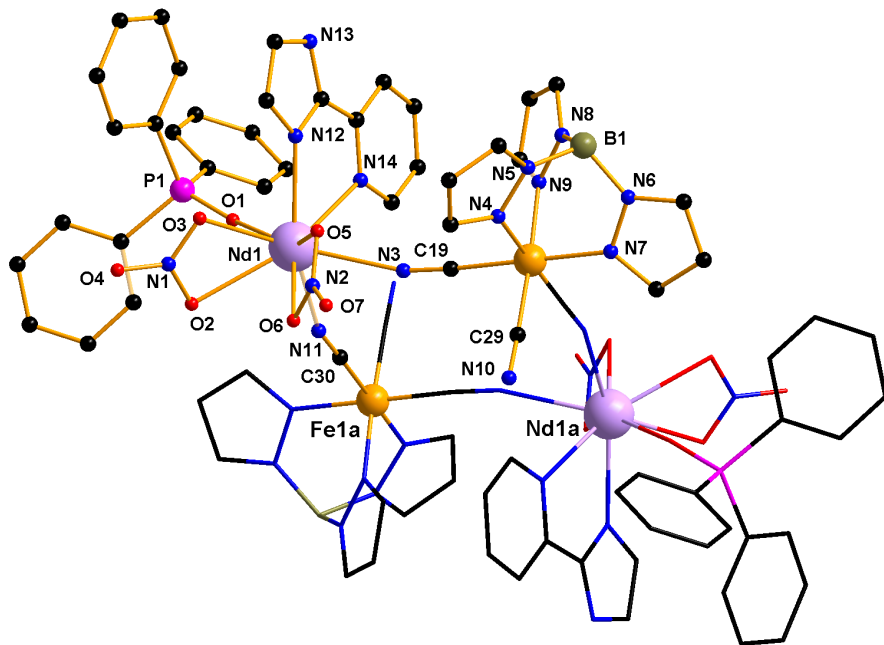


Fig. S16. View of the square-shaped cyanido-bridged heterometallic unit in **3** together with the atom labelling scheme (the molecular fragment generated by the inversion symmetry operation is represented as wires and sticks) [symmetry code (*a*) = 1-*x*, 1-*y*, 1-*z*].

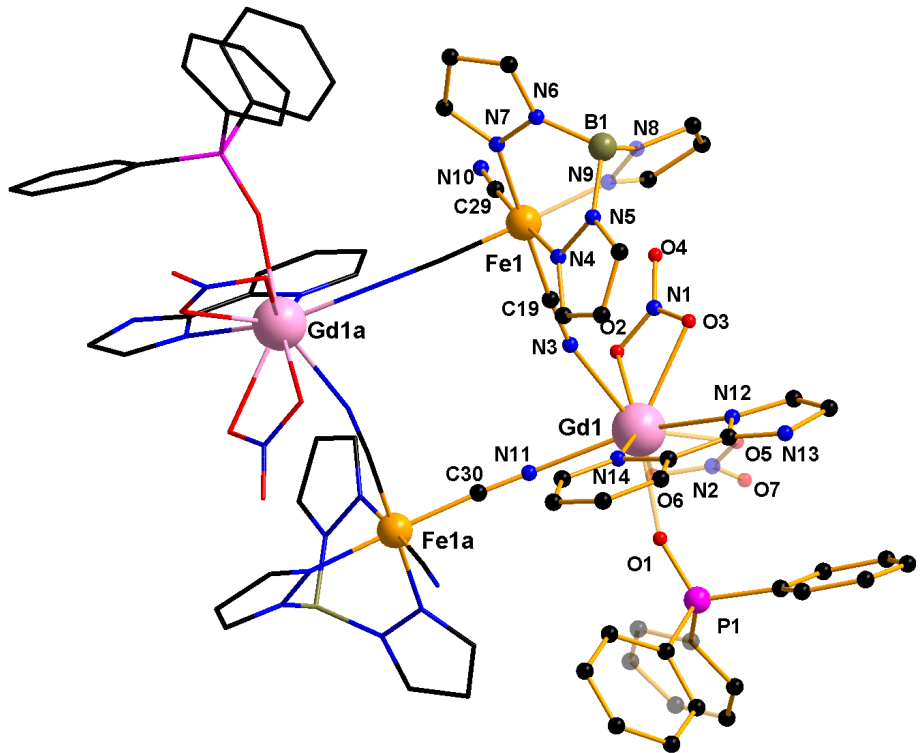


Fig. S17. View of the square-shaped cyanido-bridged heterometallic unit in **4** together with the atom labelling scheme (the molecular fragment generated by the inversion symmetry operation is represented as wires and sticks) [symmetry code (*a*) = 1-*x*, 1-*y*, 1-*z*].

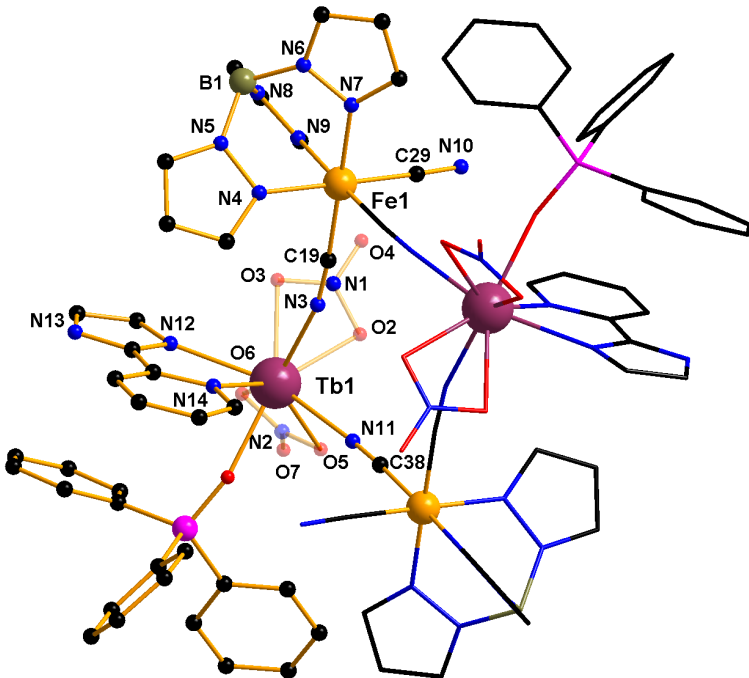


Fig. S18. View of the square-shaped cyanido-bridged heterometallic unit in **5** together with the atom labelling scheme (the molecular fragment generated by the inversion symmetry operation is represented as wires and sticks) [symmetry code (*a*) = 1-*x*, 1-*y*, 1-*z*].

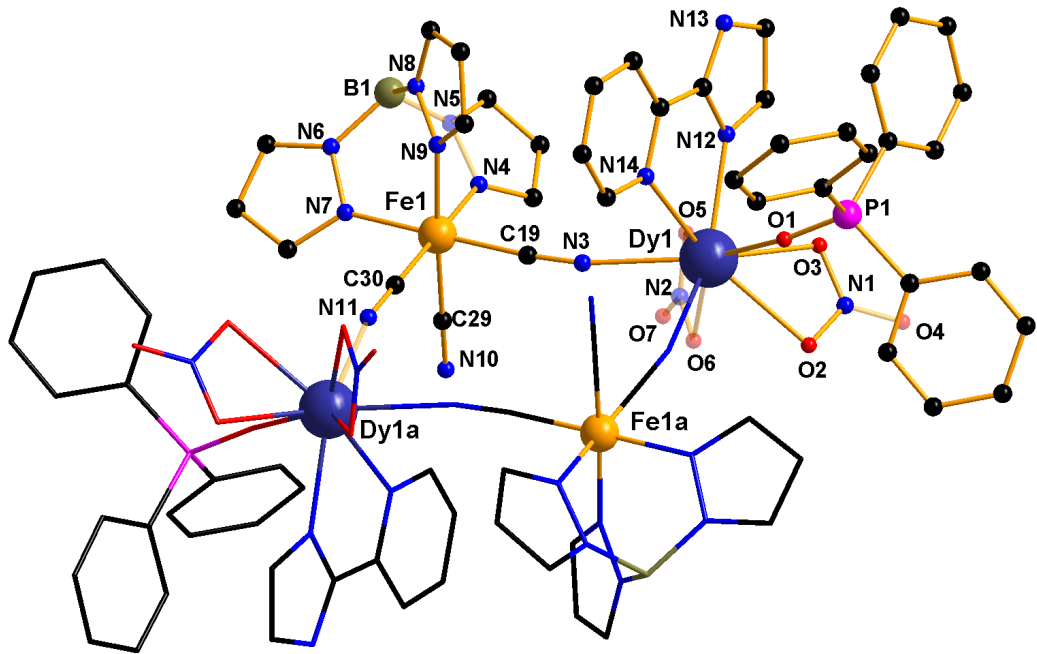


Fig. S19. View of the square-shaped cyanido-bridged heterometallic unit in **6** together with the atom labelling scheme (the molecular fragment generated by the inversion symmetry operation is represented as wires and sticks) [symmetry code (*a*) = 1-*x*, 1-*y*, 1-*z*].

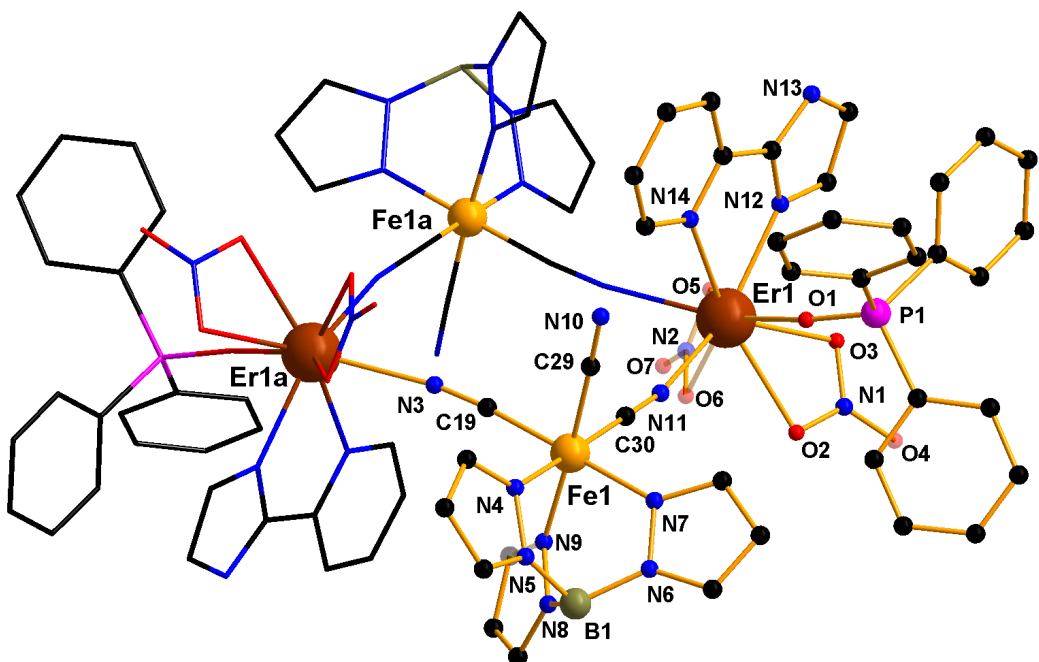


Fig. S20. View of the square-shaped cyanido-bridged heterometallic unit in **6** together with the atom labelling scheme (the molecular fragment generated by the inversion symmetry operation is represented as wires and sticks) [symmetry code (*a*) = 1-*x*, 1-*y*, 1-*z*].

Table S1. Bond Lengths (\AA) of the environments of the iron(III) and lanthanide(III) ions in **1-7**

	1	2	3	4	5	6	7
Fe1-N4	1.980(2)	1.990(10)	1.988(3)	1.9848(17)	1.9884(16)	1.968(5)	1.970(5)
Fe1-N7	1.977(2)	1.976(8)	1.975(3)	1.9719(17)	1.9718(16)	1.966(5)	1.964(5)
Fe1-N9	1.971(2)	1.955(10)	1.973(3)	1.970(2)	1.9693(16)	1.972(5)	1.972(6)
Fe1-C19	1.926(3)	1.941(12)	1.937(3)	1.922(2)	1.925(2)	1.926(7)	1.928(8)
Fe1-C29	1.933(3)	1.938(14)	1.937(4)	1.929(2)	1.934(2)	1.937(7)	1.935(7)
Fe1-C30a*	1.920(2)	1.930(12)	1.934(4)	1.929(2)	1.9296(19)	1.920(7)	1.940(8)
Ln1-N3	2.598(3)	2.550(9)	2.553(3)	2.4939(19)	2.4783(16)	2.472(6)	2.433(6)
Ln1-N11	2.608(2)	2.593(9)	2.569(3)	2.4926(18)	2.4831(16)	2.459(5)	2.435(6)
Ln1-N12	2.562(2)	2.525(9)	2.523(3)	2.480(2)	2.4569(16)	2.442(5)	2.422(6)
Ln1-N14	2.681(2)	2.686(11)	2.650(3)	2.587(2)	2.5855(16)	2.573(5)	2.543(5)
Ln1-O1	2.395(2)	2.386(8)	2.357(2)	2.3287(16)	2.3039(13)	2.296(4)	2.282(4)
Ln1-O2	2.663(2)	2.648(8)	2.636(2)	2.565(2)	2.5724(15)	2.555(5)	2.530(5)
Ln1-O3	2.577(2)	2.563(8)	2.524(3)	2.4805(18)	2.4705(14)	2.448(4)	2.422(5)
Ln1-O5	2.603(2)	2.606(9)	2.568(2)	2.5227(17)	2.5170(13)	2.503(4)	2.491(5)
Ln1-O6	2.534(2)	2.517(10)	2.498(2)	2.4542(19)	2.4347(14)	2.421(4)	2.401(4)

*Symmetry code: $(a) = 1-x, 1-y, 1-z$

Table S2. Bond Angles ($^{\circ}$) of the environments of the iron(III) and lanthanide(III) ions in **1-7**

	1	2	3	4	5	6	7
N4-Fe1-N7	88.25(9)	88.1(4)	88.25(11)	88.24(7)	88.27(6)	89.6(2)	89.5(2)
N4-Fe1-N9	87.10(9)	87.1(4)	87.37(12)	87.11(8)	87.28(7)	87.1(2)	88.7(2)
N7-Fe1-N9	89.85(10)	89.9(4)	90.04(12)	89.98(8)	89.88(7)	88.0(2)	87.1(2)
Fe1-C19-N3	176.3(2)	175.8(11)	176.1(3)	175.58(19)	175.43(17)	175.1(6)	174.8(6)
Fe1-C29-N10	176.9(2)	179.1(12)	176.8(3)	177.1(2)	177.02(18)	176.6(6)	175.9(7)
Fe1-C30a-N11a*	177.7(2)	176.0(10)	177.2(3)	177.08(18)	176.99(17)	177.1(6)	177.0(6)
N4-Fe1-C19	91.82(10)	91.4(5)	91.56(13)	91.56(8)	91.55(7)	91.6(3)	91.2(3)
N4-Fe1-C29	89.88(10)	88.5(5)	89.46(13)	89.61(8)	89.29(7)	89.6(2)	89.4(3)
N4-Fe1-C30a*	178.75(10)	178.8(4)	178.72(13)	178.36(8)	178.36(7)	178.2(3)	178.0(2)
N7-Fe1-C19	179.89(12)	179.2(6)	179.71(14)	179.42(8)	179.68(8)	179.4(3)	179.3(2)
N7-Fe1-C29	91.53(11)	91.4(4)	91.48(13)	91.55(9)	91.68(7)	91.9(3)	92.0(3))
N7-Fe1-C30a*	90.76(10)	91.0(4)	90.62(12)	90.98(8)	90.83(7)	90.8(3)	91.0(3)
N9-Fe1-C19	90.07(11)	90.7(5)	90.16(13)	89.46(9)	89.86(7)	90.0(3)	89.8(2)
N9-Fe1-C29	176.64(10)	175.3(5)	176.44(13)	176.33(8)	176.19(7)	176.3(2)	176.2(3)
N9-Fe1-C30a*	93.66(10)	93.7(5)	93.23(13)	94.35(8)	94.10(7)	94.3(2)	94.9(2)
C19-Fe1-C29	88.56(12)	88.0(5)	88.30(14)	88.99(9)	88.58(8)	88.5(3)	88.6(3)
C19-Fe1-C30a*	89.17(11)	89.5(5)	89.57(13)	89.23(8)	89.36(8)	89.6(3)	89.1(3)
C29-Fe1-C30a*	89.38(11)	90.7(5)	89.97(14)	88.96(9)	89.36(8)	89.0(3))	88.6(3)
N12-Ln1-N14	62.67(7)	63.2(3)	63.76(9)	64.90(7)	65.16(5)	65.48(16)	66.0(2)
Ln1-N3-C19	162.5(2)	162.5(9)	162.3(3)	165.82(17)	165.22(15)	166.4(5)	166.2(6)
Ln1-N11-C30	161.6(2)	162.5(9)	161.9(3)	164.83(17)	164.79(15)	166.0(5)	166.6(5)
O2-Ln1-O1	73.13(7)	72.9(3)	72.09(8)	72.58(6)	72.19(5)	71.97(15)	71.98(15)
O2-Ln1-O3	48.55(6)	49.1(2)	49.26(8)	50.12(6)	50.45(5)	51.09(15))	51.07(17)
O2-Ln1-O5	97.15(7)	97.3(3)	98.53(8)	98.67(6)	99.62(5)	100.21(15)	100.54(16)
O2-Ln1-O6	66.86(7)	66.7(3)	66.47(8)	66.68(7)	66.42(5)	66.53(16)	66.43(16)
O2-Ln1-N3	135.66(8)	135.7(3)	135.54(9)	134.27(6)	134.35(5)	134.33(17)	134.17(17)
O2-Ln1-N11	84.80(7)	84.4(3)	83.86(8)	80.40(6)	80.55(5)	79.61(17)	79.04(18)
O2-Ln1-N12	117.43(7)	117.8(3)	118.02(8)	120.48(6)	120.38(5)	121.07(17)	121.50(18)
O2-Ln1-N14	146.26(7)	145.6(3)	145.04(8)	144.51(6)	145.15(5)	143.60(16)	143.19(17)
O3-Ln1-O1	79.99(8)	80.3(3)	80.02(8)	78.18(6)	79.02(5)	78.85(15)	78.33(17)
O3-Ln1-O5	70.29(8)	69.7(3)	70.37(8)	70.52(6)	70.40(5)	70.19(16)	70.70(17)
O3-Ln1-O6	79.08(8)	79.2(3)	78.22(8)	79.68(7)	78.78(5)	78.82(16)	78.97(17)
O3-Ln1-N3	140.08(8)	140.0(3)	140.04(9)	140.35(6)	140.02(5)	139.56(16)	140.43(18)
O3-Ln1-N11	132.73(7)	132.9(3)	132.65(8)	130.00(6)	130.62(5)	130.34(17)	129.74(18)
O3-Ln1-N12	70.67(7)	70.5(3)	70.89(8)	72.18(6)	72.10(5)	72.22(16)	72.62(18)
O3-Ln1-N14	127.59(7)	127.8(3)	128.75(8)	130.20(6)	130.77(5)	131.12(16)	131.65(18)
O5-Ln1-O6	49.64(7)	50.2(3)	50.49(8)	51.01(6)	51.60(5)	52.00(15)	52.23(16)
O5-Ln1-O1	146.44(7)	146.3(3)	146.51(8)	144.33(6)	144.90(5)	144.35(15)	144.16(17)
O5-Ln1-N3	69.88(8)	70.4(3)	69.81(9)	70.01(6)	69.85(5)	69.59(16)	69.98(18)

O5-Ln1-N11	132.98(7)	133.3(3)	132.91(8)	132.91(6)	132.85(5)	133.20(16)	132.98(17)
O5-Ln1-N12	71.42(7)	71.0(3)	71.32(8)	70.84(6)	70.87(5)	70.40(16)	70.40(17)
O5-Ln1-N14	113.03(7)	113.8(3)	113.55(8)	114.93(6)	114.57(5)	114.61(16)	114.94(17)
O6-Ln1-O1	139.36(7)	138.9(3)	138.03(8)	138.96(6)	138.29(5)	138.26(16)	138.20(16)
O6-Ln1-N3	73.41(8)	73.6(3)	74.22(9)	72.90(7)	73.52(5)	73.44(17)	73.73(18)
O6-Ln1-N11	90.24(8)	89.8(3)	89.95(9)	87.70(6)	87.80(5)	87.56(16)	87.11(18)
O6-Ln1-N12	119.97(7)	120.3(3)	120.46(8)	121.05(6)	121.42(5)	121.42(16)	121.64(19)
O6-Ln1-N14	145.30(7)	145.7(3)	146.12(8)	144.69(6)	145.15(5)	144.96(17)	144.84(18)
N3-Ln1-N11	76.28(8)	76.3(3)	75.97(9)	77.45(7)	76.85(5)	77.59(18))	77.2(2)
N3-Ln1-N12	98.85(8)	98.7(3)	99.16(9)	98.09(7)	98.57(5)	97.95(18))	98.09(19)
N3-Ln1-N14	72.09(8)	72.2(3)	71.98(9)	71.80(6)	71.63(5)	71.54(17)	71.15(18)
N3-Ln1-O1	138.75(7)	138.5(3)	138.93(9)	140.28(6)	139.90(5)	140.39(16)	140.11(17)
N11-Ln1-N12	147.12(8)	147.3(4)	147.13(9)	148.67(6)	148.31(6)	148.56(17)	148.77(19)
N11-Ln1-N14	85.26(7)	84.8(3)	84.17(9)	84.54(7)	83.94(5)	83.86(17)	83.55(19)
N11-Ln1-O1	79.11(7)	78.9(3)	79.14(9)	80.80(6)	80.57(5)	80.74(17)	81.14(17)
N12-Ln1-O1	84.53(8)	85.0(3)	84.67(9)	83.83(6)	83.86(5)	83.87(17)	83.66(18)
N14-Ln1-O1	73.35(7)	73.0(3)	73.44(8)	73.39(6)	73.39(5)	73.51(16)	73.46(17)

Table S3. Summary of the SHAPE analysis for the $[LnN_4O_5]$ fragment in **1-7** [$Ln = Ce$ (**1**), Pr (**2**), Nd (**3**), Gd (**4**), Tb (**5**), Dy (**6**) and Er (**7**)]^a

CN = 9 ^b	Ce(III)	Pr(III)	Nd(III)	Gd(III)	Tb(III)	Dy(III)	Er(III)
EP-9	34.592	34.417	34.310	34.591	34.409	34.311	34.294
OPY-9	22.475	22.615	22.244	22.850	22.619	22.652	22.699
HBPY-9	17.680	17.670	17.780	17.926	18.104	18.086	18.057
JTC-9	15.743	15.525	15.648	15.379	15.326	15.239	15.197
JCCU-9	9.045	9.050	8.852	8.997	8.859	8.866	8.799
CCU-9	7.755	7.762	7.657	7.839	7.764	7.809	7.751
JCSAPR-9	3.485	3.430	3.204	2.955	2.804	2.695	2.629
CSAPR-9	2.526	2.476	2.330	2.093	2.000	1.915	1.859
JTCTPR-9	4.396	4.170	4.088	3.688	3.552	3.396	3.296
TCTPR-9	3.434	3.338	3.248	2.759	2.745	2.629	2.526
JTDIC-9	12.696	12.631	12.535	13.277	13.217	13.374	13.209
HH-9	11.725	11.738	11.652	11.458	11.767	11.804	11.693
MFF-9	1.364	1.312	1.383	1.159	1.237	1.202	1.196

^aThe listed values correspond to the deviation between the ideal and real coordination polyhedra, the lowest values being given in bold. ^bEP-9, D_{9h} , enneagon; OPY-9, C_{8v} , octagonal pyramid; HBPY-9, D_{7h} , heptagonal bipyramid; JTC-9, C_{3v} , Johnson triangular cupola J3; JCCU-9, C_{4v} , capped cube J8; CCU-9, C_{4v} , spherical-relaxed capped cube; JCSAPR-9, C_{4v} , capped square antiprism; CSAPR-9, C_{4v} , spherical capped square antiprism; JTCTPR-9, D_{3h} , tricapped trigonal prism J51; TCTPR-9, D_{3h} , spherical tricapped trigonal prism; JTDIC-9, C_{3v} , tridiminished icosahedron; HH-9, C_{2v} , hula-hoop; MFF-9, C_s , muffin.

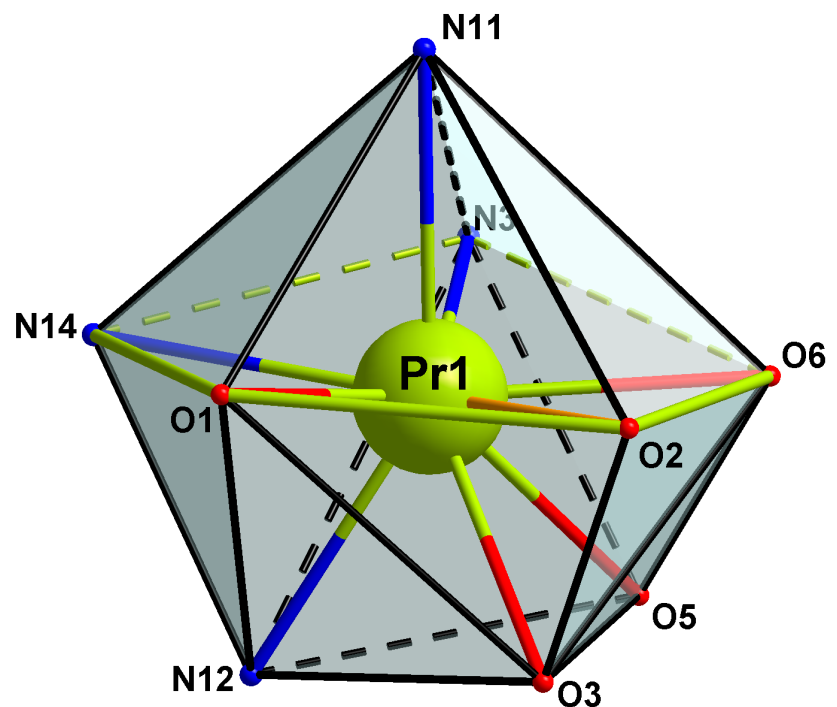


Fig. S21. Muffin-like geometry in 2.

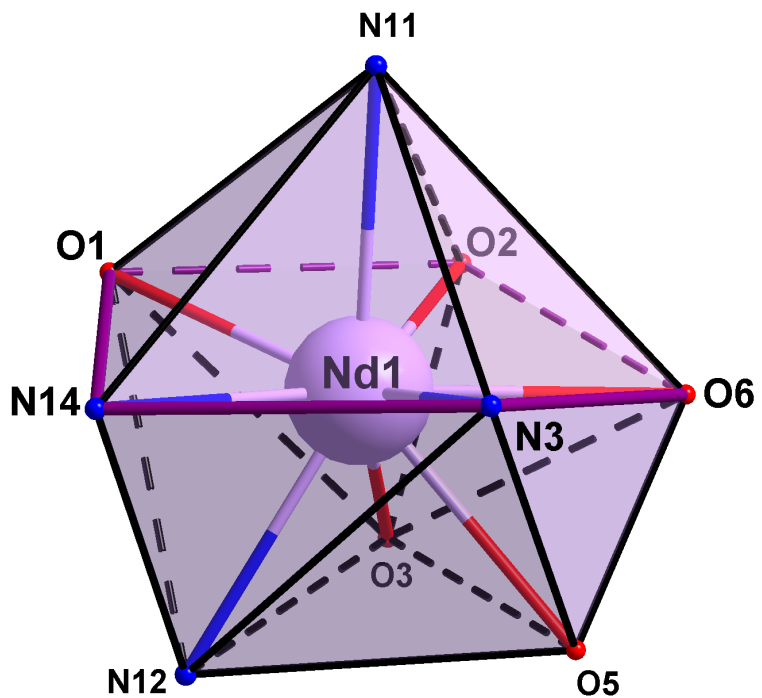


Fig. S22. Muffin-like geometry in 3.

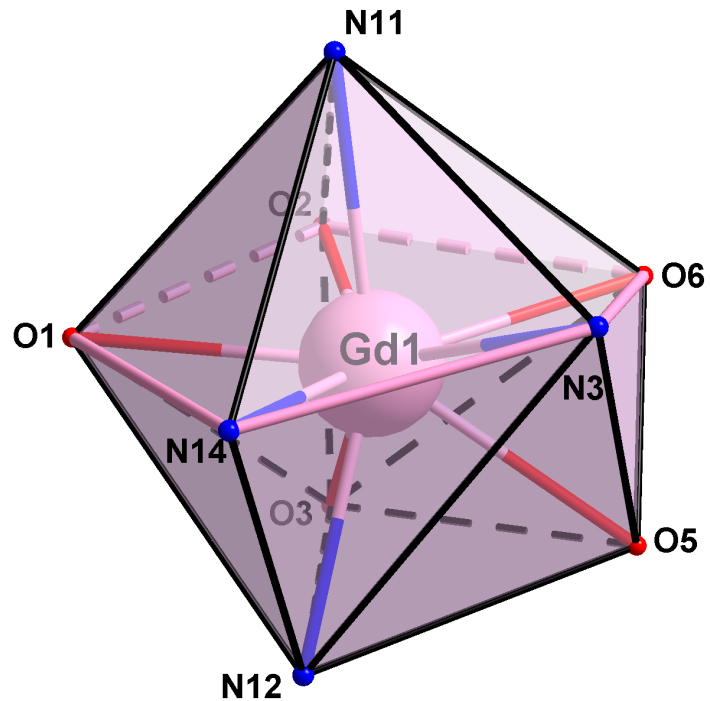


Fig. S23. Muffin-like surrounding in 4.

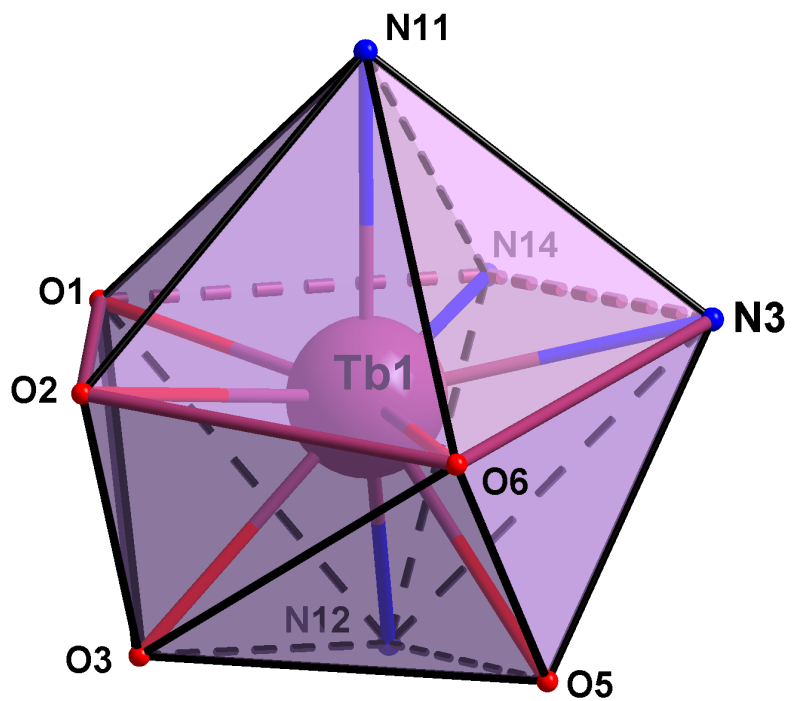


Fig. S24. Muffin-like surrounding in 5.

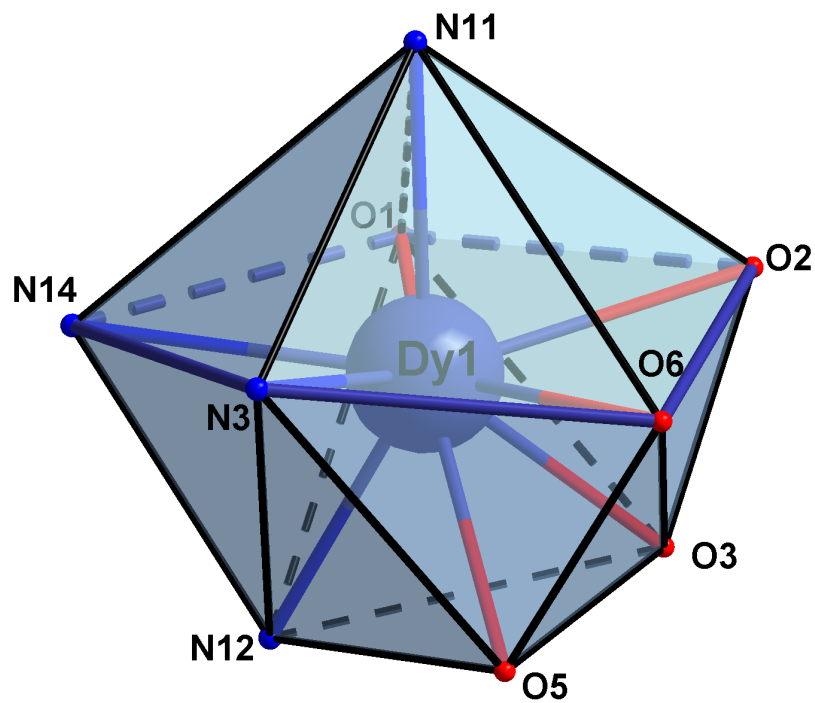


Fig. S25. Muffin-like surrounding in 6.

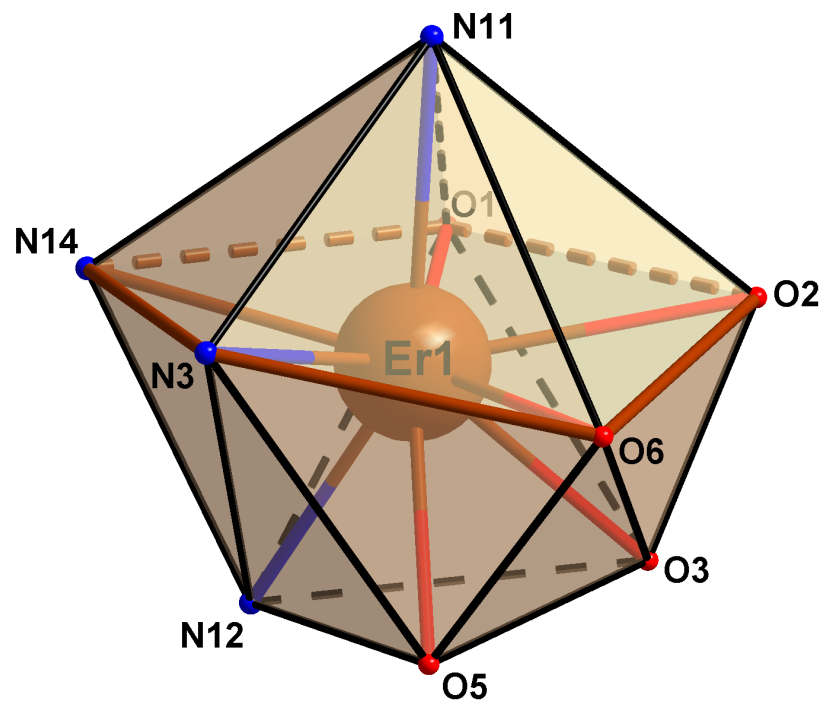


Fig. S26. Muffin-like geometry in 7.

Table S4. Selected intermolecular contacts for **1-7***

Compound	D-H···A	D-H (Å)	H···A (Å)	D···A (Å)	Angle D-H···A
1		0.84(5)	2.36(5)	3.131(4)	153(4)
		0.84(5)	2.30(5)	2.956(4)	135(4)
2		0.86	2.34	3.145(14)	157
		0.86	2.23	2.912(15)	136
3	N13-H13 <i>b</i> ···O2 ^{<i>i</i>}	0.80(6)	2.42(6)	3.157(5)	155(5)
		0.80(6)	2.29(6)	2.917(5)	136(5)
4	N13-H13 <i>b</i> ···O4 ^{<i>i</i>}	0.91(4)	2.58(4)	3.413(4)	152(3)
		0.91(4)	2.07(4)	2.873(5)	146(3)
5		0.86(3)	2.63(3)	3.415(3)	153(3)
		0.86(3)	2.13(3)	2.866(3)	144(2)
6		0.860(11)	2.69(8)	3.463(9)	152(8)
		0.860(10)	2.100(9)	2.862(9)	147.3(8)
7		0.860(11)	2.79(8)	3.563(9)	149(8)
		0.860(10)	2.090(10)	2.871(10)	150.8(8)

*D = donor and A = acceptor. ^{*i*}Symmetry code: (*b*) = 1+*x*, *y*, *z*.

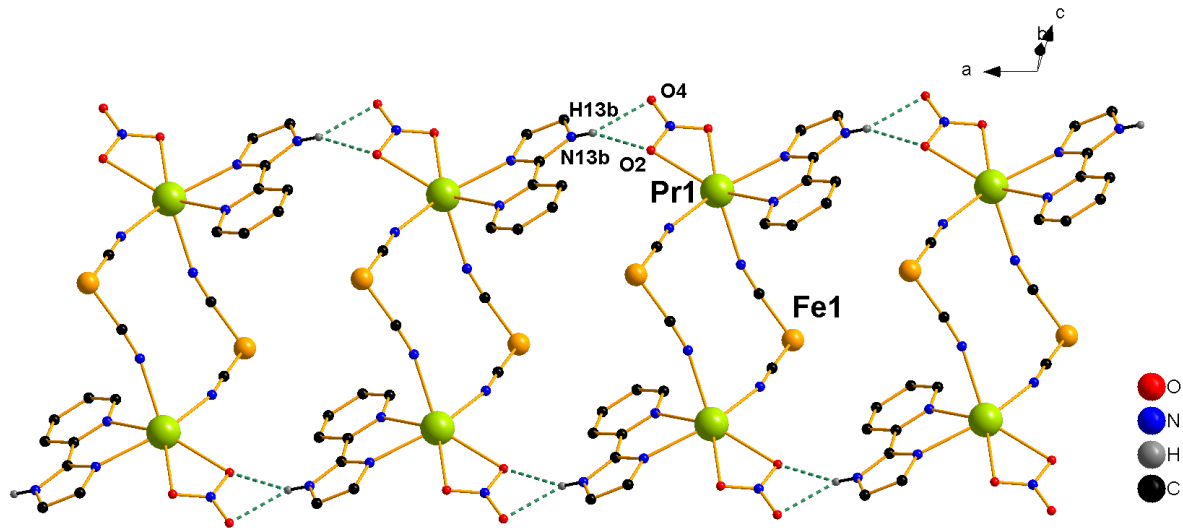


Fig. S27. View of a fragment of the supramolecular ladder-like chain running parallel to the *a* axis in **2**. The dashed lines stand for the hydrogen bonds and the Ph₃PO, {HB(pz)₃}⁻, one nitrate and the terminal cyanide ligands were omitted for the sake of clarity [symmetry code (*b*) = 1+*x*, *y*, *z*].

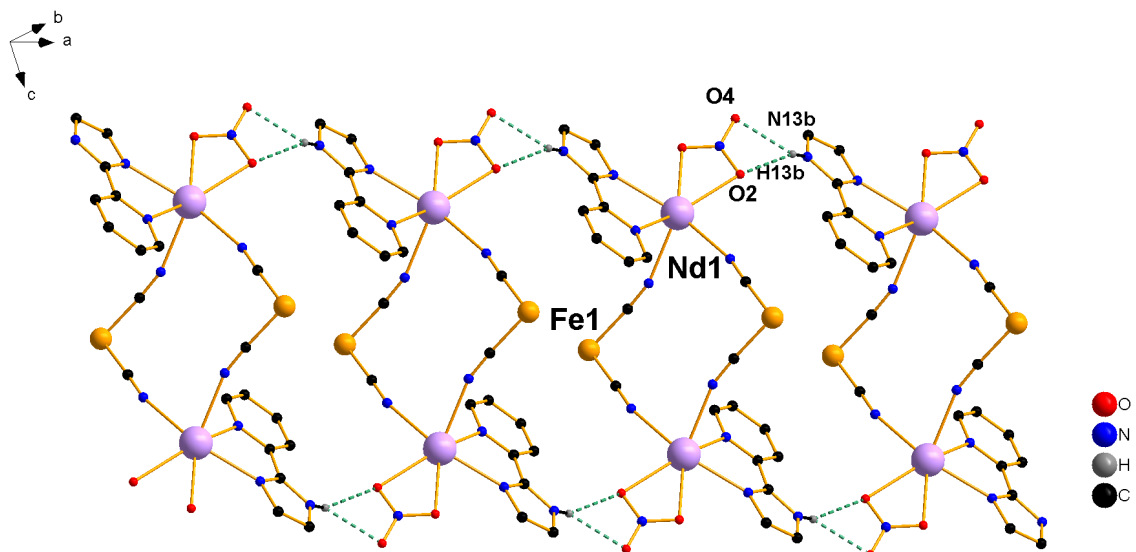


Fig. S28. View of a fragment of the supramolecular ladder-like chain running parallel to the *a* axis in **3**. The dashed lines stand for the hydrogen bonds and the Ph₃PO, {HB(pz)₃}⁻, one nitrate and the terminal cyanide ligands were omitted for the sake of clarity [symmetry code (*b*) = 1+*x*, *y*, *z*].

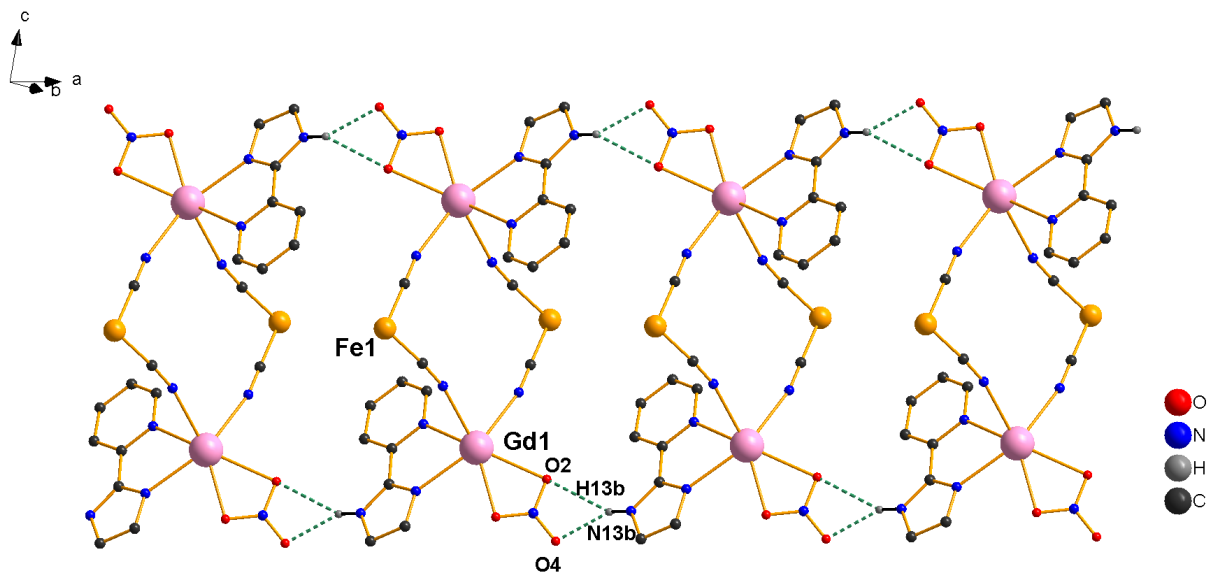


Fig. S29. View of a fragment of the supramolecular ladder-like chain running parallel to the *a* axis in **4**. The dashed lines stand for the hydrogen bonds and the Ph₃PO, {HB(pz)₃}⁻, one nitrate and the terminal cyanide ligands were omitted for the sake of clarity [symmetry code (*b*) = 1+*x*, *y*, *z*].

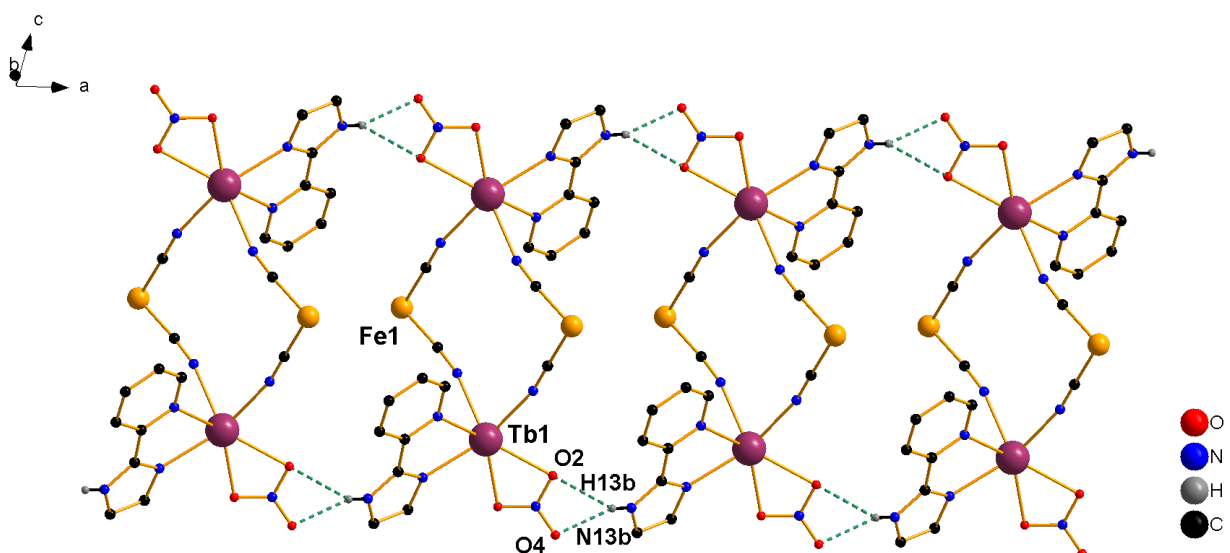


Fig. S30. View of a fragment of the supramolecular ladder-like chain running parallel to the *a* axis in **5**. The dashed lines stand for the hydrogen bonds and the Ph₃PO, {HB(pz)₃}⁻, one nitrate and the terminal cyanide ligands were omitted for the sake of clarity [symmetry code (*b*) = 1+*x*, *y*, *z*].

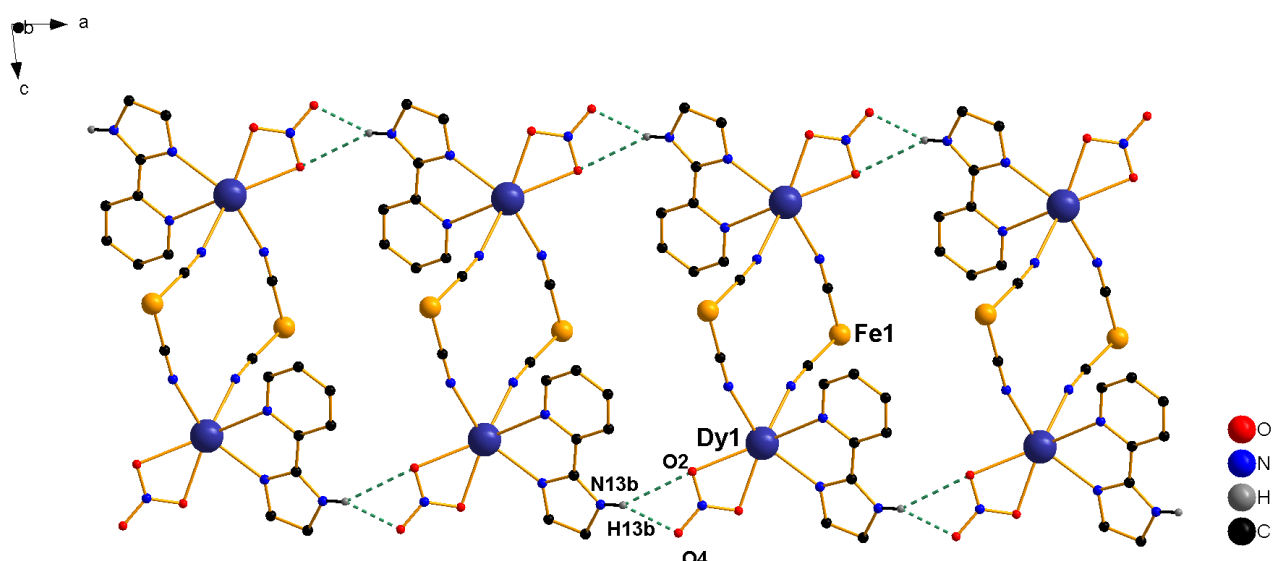


Fig. S31. View of a fragment of the supramolecular ladder-like chain running parallel to the *a* axis in **6**. The dashed lines stand for the hydrogen bonds and the Ph_3PO , $\{\text{HB}(\text{pz})_3\}^-$, one nitrate and the terminal cyanide ligands were omitted for the sake of clarity [symmetry code (*b*) = $1+x, y, z$].

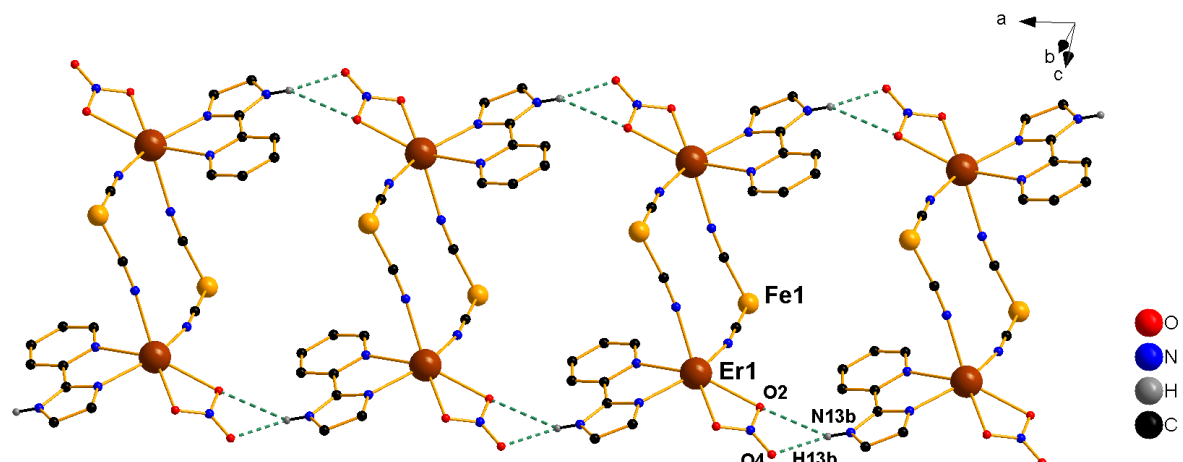


Fig. S32. View of a fragment of the supramolecular ladder-like chain running parallel to the *a* axis in **7**. The dashed lines stand for the hydrogen bonds and the Ph_3PO , $\{\text{HB}(\text{pz})_3\}^-$, one nitrate and the terminal cyanide ligands were omitted for the sake of clarity [symmetry code (*b*) = $1+x, y, z$].

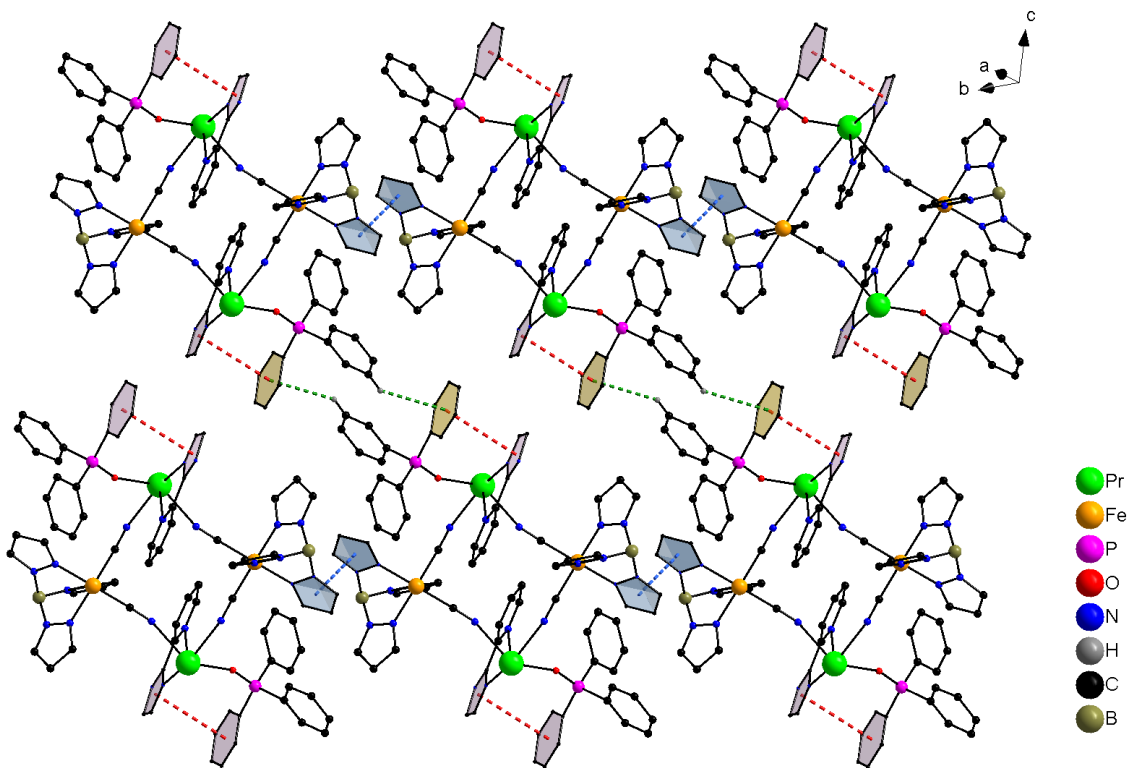


Fig. S33. Crystal packing in **2** showing the supramolecular layers which grow in the crystallographic bc plane, through $\pi-\pi$ stacking (blue and red dotted lines) and C-H... π (green dotted lines) interactions involving imidazolyl, pyrazolyl and phenyl rings of pyim, $\{\text{HB(pz)}_3\}^-$ and Ph_3PO ligands from adjacent squares. The nitrate groups and the terminal cyanide ligands were removed for the sake of clarity.

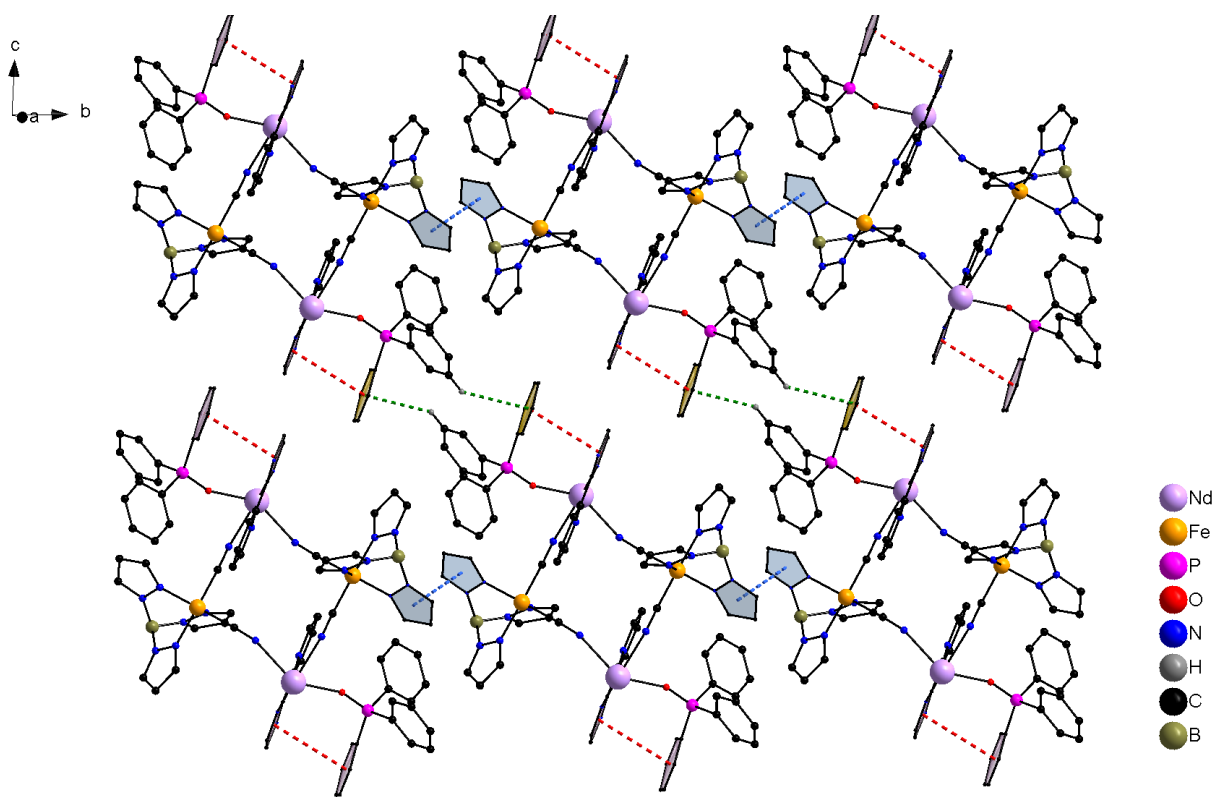


Fig. S34. Crystal packing in **3** showing the supramolecular layers which grow in the crystallographic bc plane, through $\pi-\pi$ stacking (blue and red dotted lines) and C-H $\cdots\pi$ (green dotted lines) interactions involving imidazolyl, pyrazolyl and phenyl rings of pyim, $\{\text{HB}(\text{pz})_3\}^-$ and Ph_3PO ligands from adjacent squares. The nitrate groups and the terminal cyanide ligands were removed for the sake of clarity.

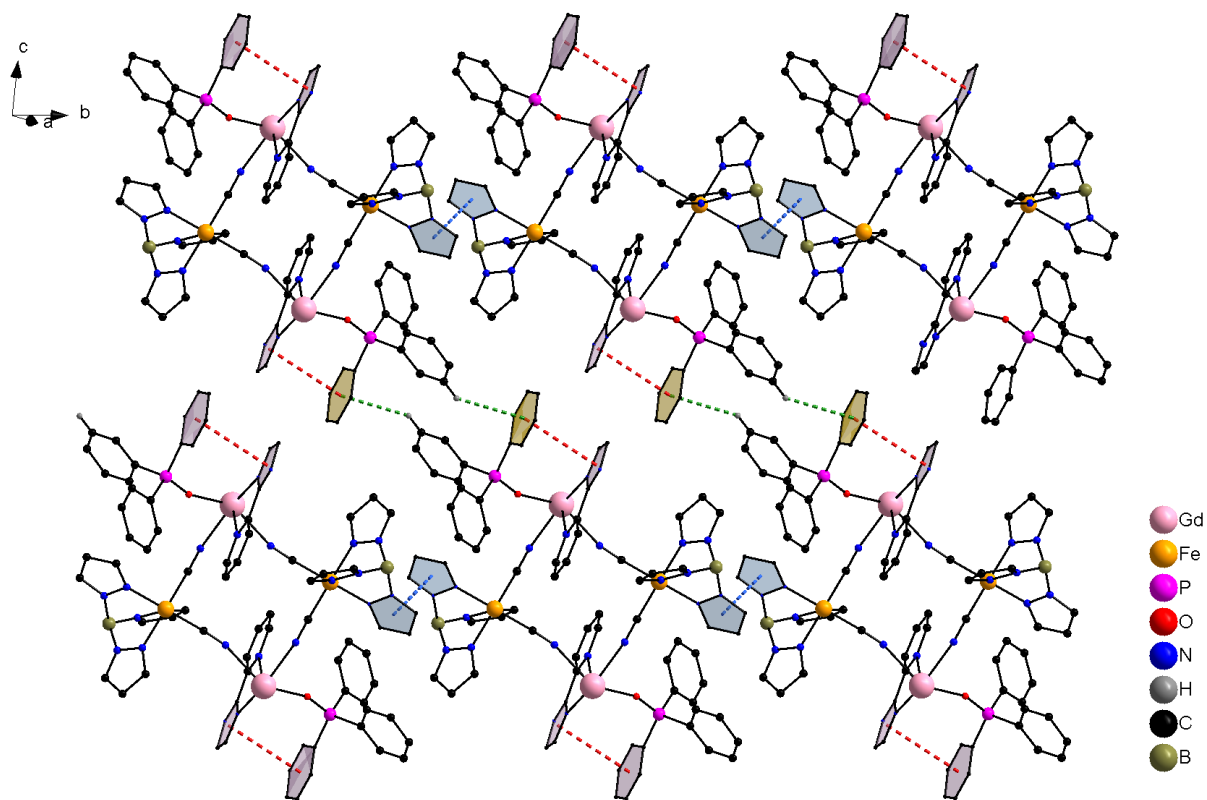


Fig. S35. Crystal packing in **4** showing the supramolecular layers which grow in the crystallographic *bc* plane, through $\pi\text{-}\pi$ stacking (blue and red dotted lines) and C-H... π (green dotted lines) interactions involving imidazolyl, pyrazolyl and phenyl rings of pyim, $\{\text{HB(pz)}_3\}^-$ and Ph_3PO ligands from adjacent squares. The nitrate groups and the terminal cyanide ligands were removed for the sake of clarity.

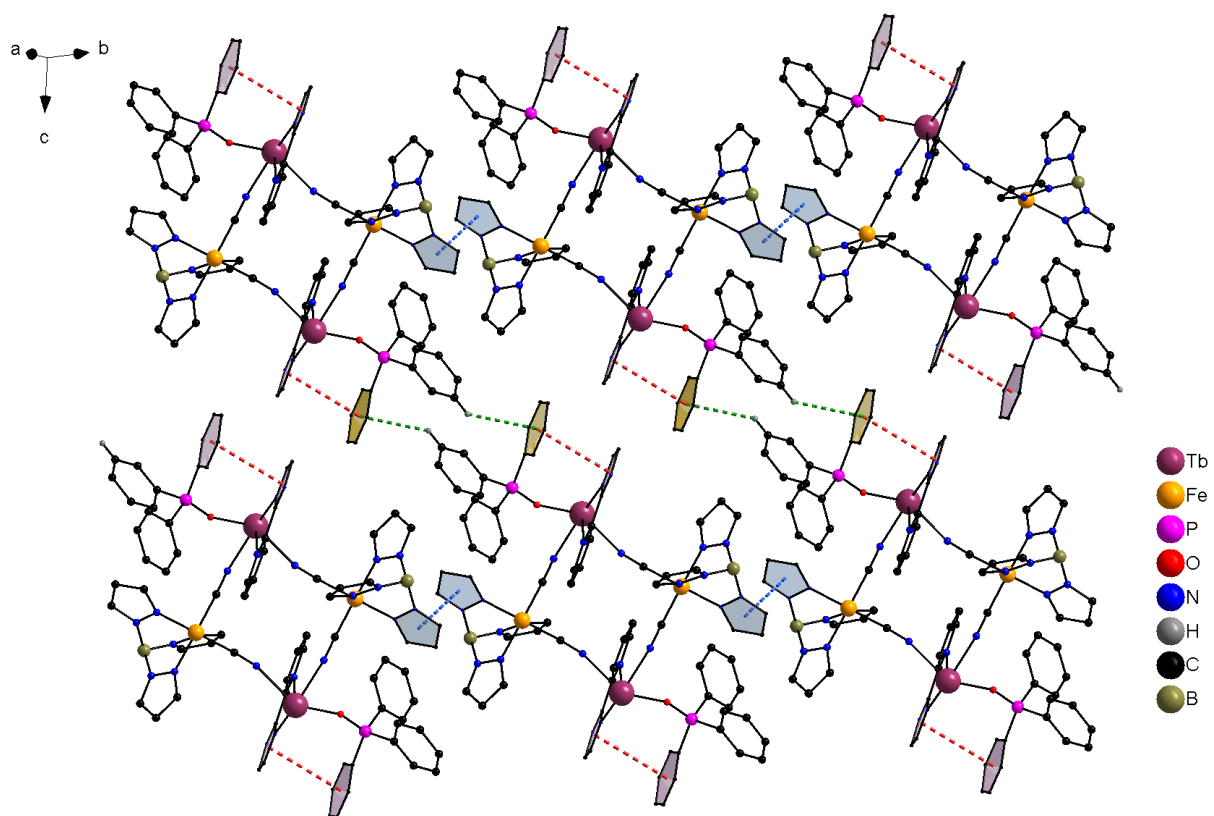


Fig. S36. Crystal packing in **5** showing the supramolecular layers which grow in the crystallographic *bc* plane, through $\pi-\pi$ stacking (blue and red dotted lines) and C-H $\cdots\pi$ (green dotted lines) interactions involving imidazolyl, pyrazolyl and phenyl rings of pyim, $\{\text{HB(pz)}_3\}^-$ and Ph_3PO ligands from adjacent squares. The nitrate groups and the terminal cyanide ligands were removed for the sake of clarity.

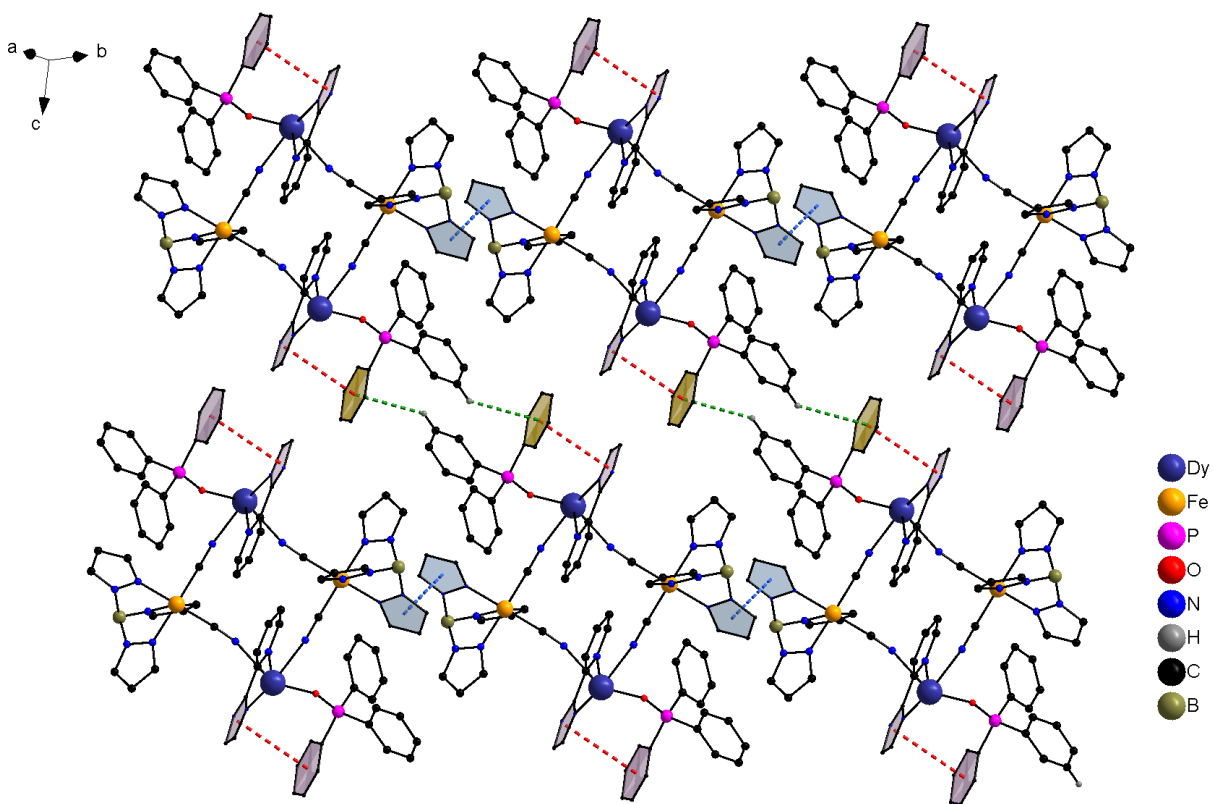


Fig. S37. Crystal packing in **6** showing the supramolecular layers which grow in the crystallographic *bc* plane, through π - π stacking (blue and red dotted lines) and C-H \cdots π (green dotted lines) interactions involving imidazolyl, pyrazolyl and phenyl rings of pyim, $\{\text{HB(pz)}_3\}^-$ and Ph₃PO ligands from adjacent squares. The nitrate groups and the terminal cyanide ligands were removed for the sake of clarity.

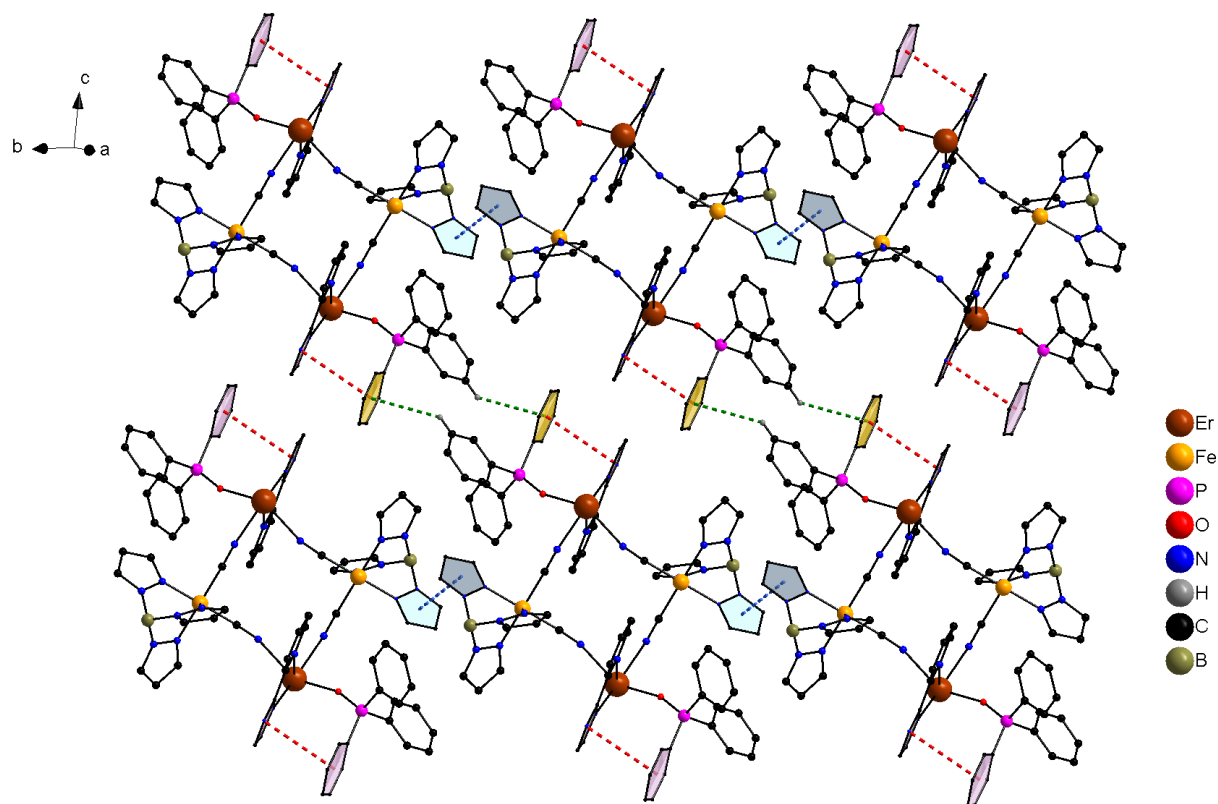


Fig. S38. Crystal packing in **7** showing the supramolecular layers which grow in the crystallographic *bc* plane, through π - π stacking (blue and red dotted lines) and C-H... π (green dotted lines) interactions involving imidazolyl, pyrazolyl and phenyl rings of pyim, $\{\text{HB(pz)}_3\}^-$ and Ph_3PO ligands from adjacent squares. The nitrate groups and the terminal cyanide ligands were removed for the sake of clarity.

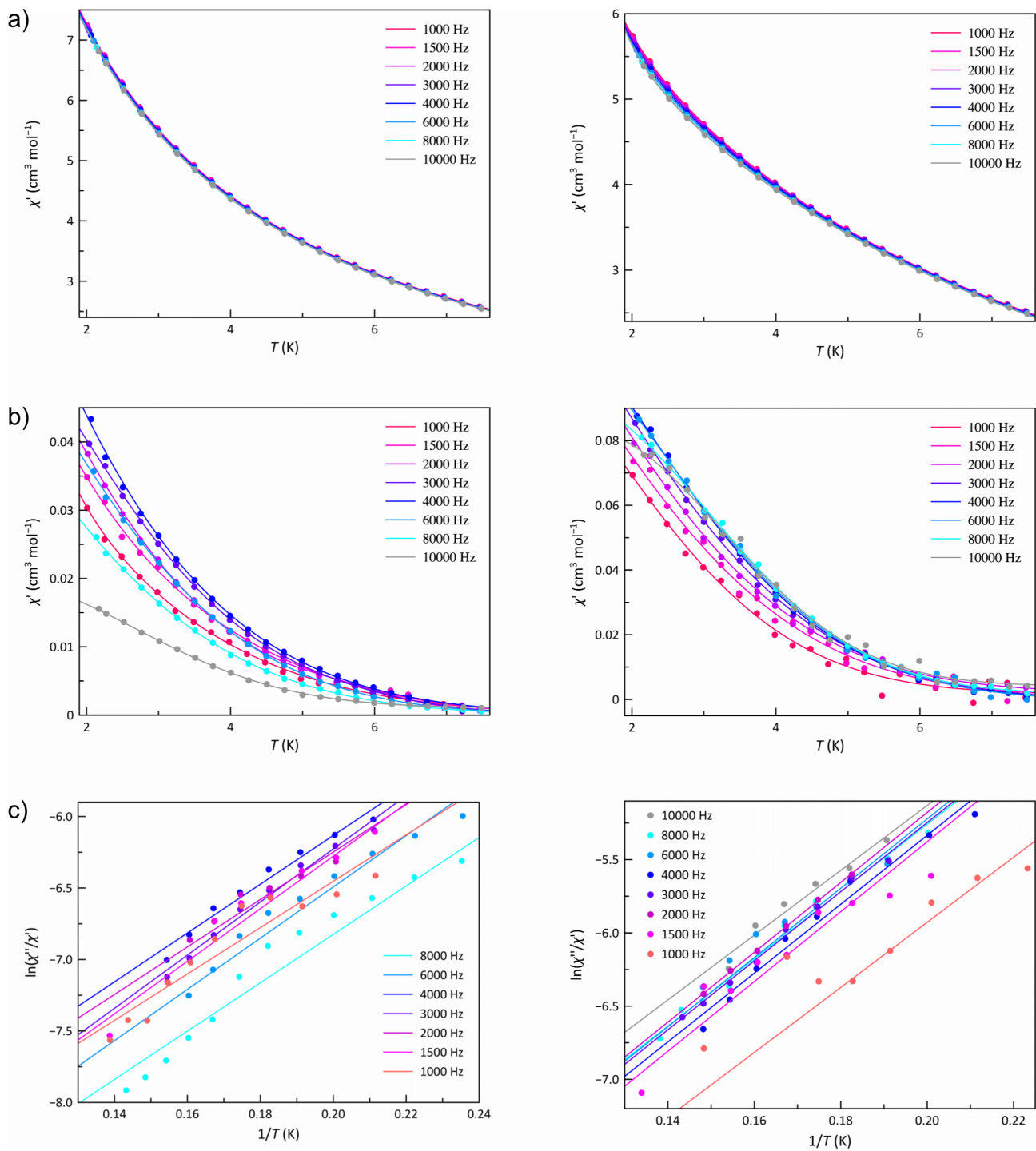


Fig. S39. Temperature dependence of (a) χ_M' , (b) χ_M'' , and (c) $\ln(\chi''/\chi')$ for **5** at a ± 5.0 G oscillating field in the frequency range of 1.0–10.0 kHz under applied static magnetic fields of 1.0 (left) and 2.5 kOe (right). The solid lines are only eye-guides in (a) and (b), and best-fit curves in (c).

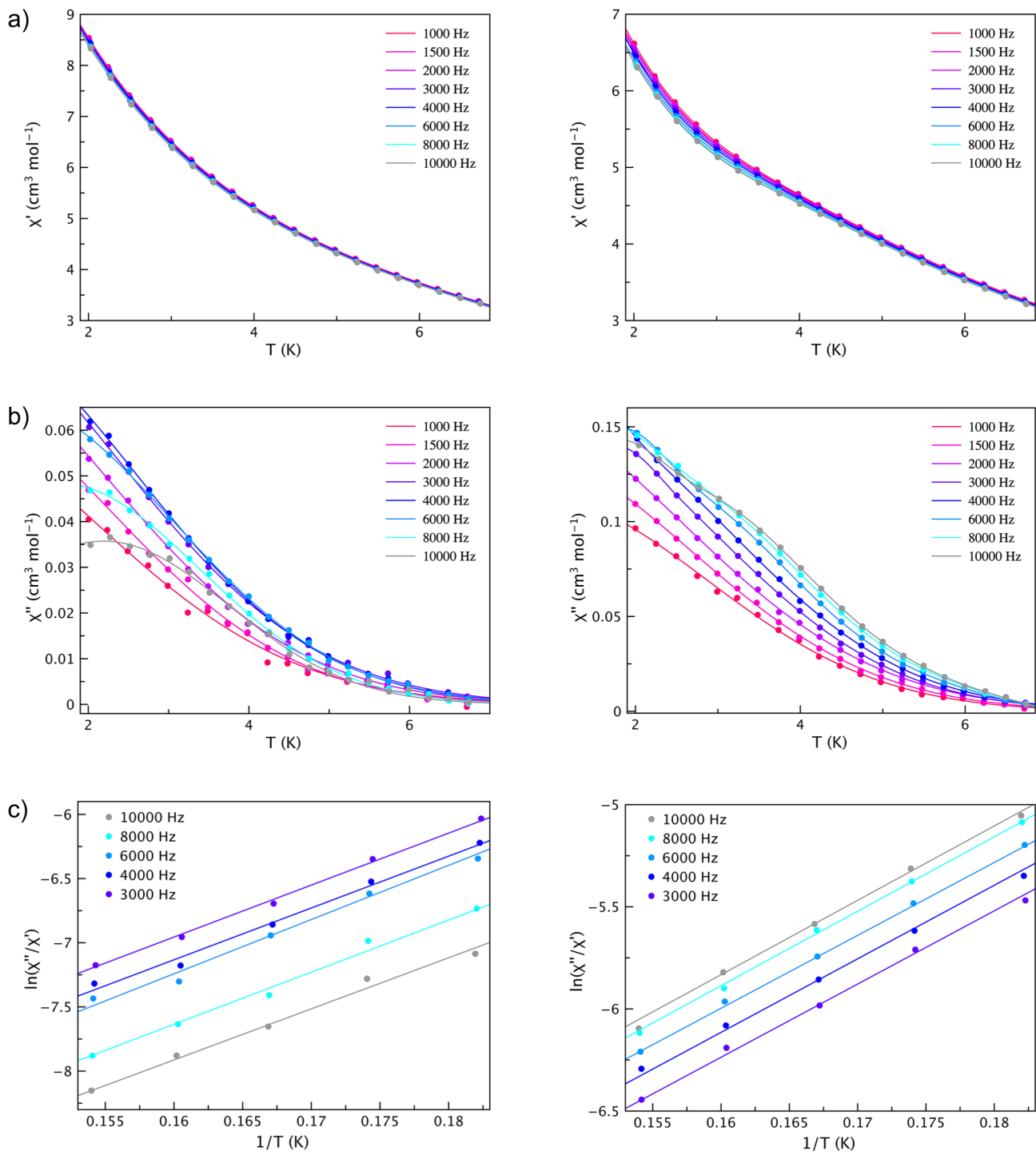


Fig. S40. Temperature dependence of (a) χ_M' , (b) χ_M'' , and (c) $\ln(\chi_M''/\chi_M')$ for **6** at a ± 5.0 G oscillating field in the frequency range of 1.0–10.0 kHz under applied static magnetic fields of 1.0 (left) and 2.5 kOe (right). The solid lines are only eye-guides in (a) and (b), and best-fit curves in (c).

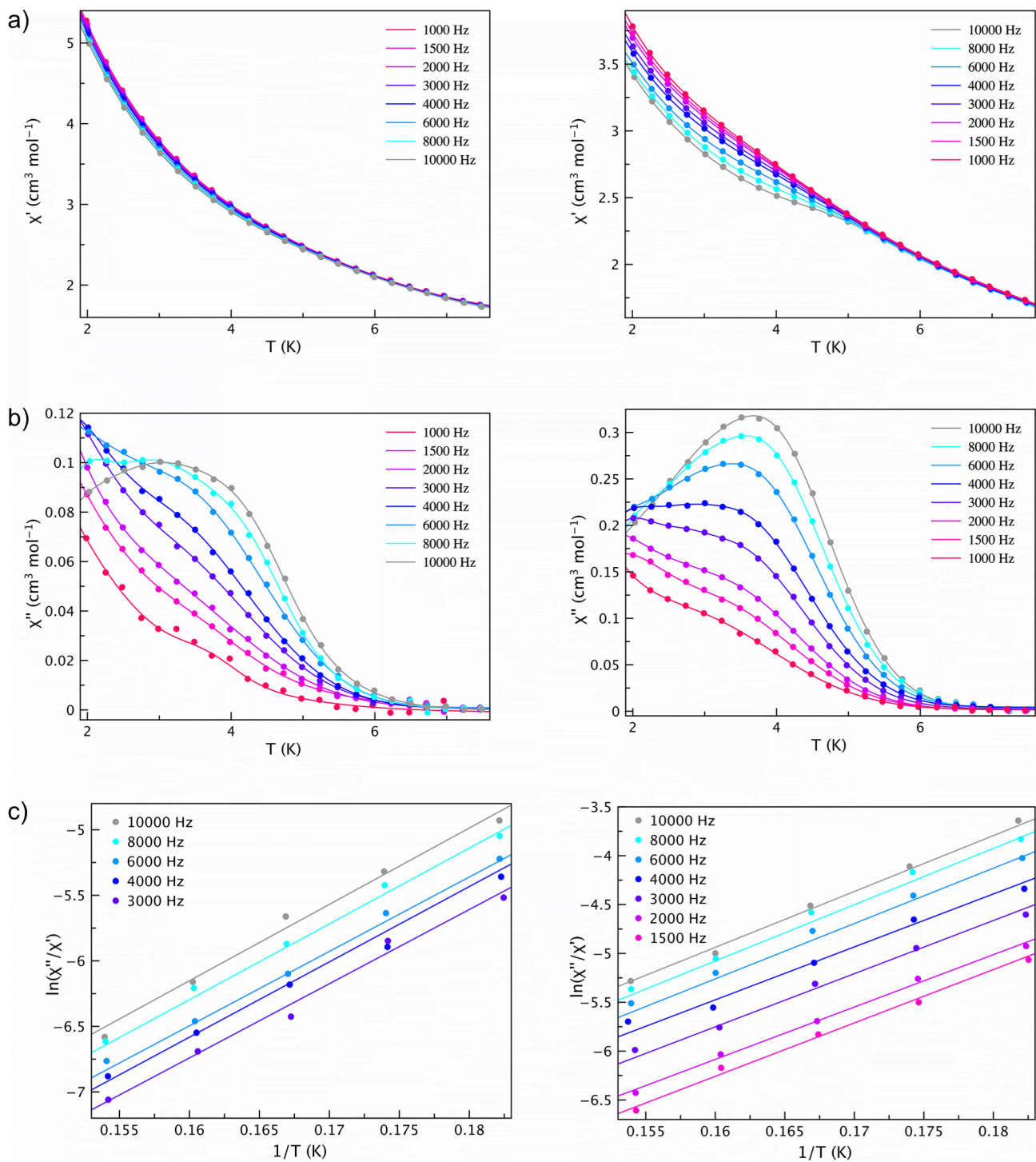


Fig. S41. Temperature dependence of (a) χ_M' , (b) χ_M'' , and (c) $\ln(\chi_M''/\chi_M')$ for **7** at a ± 5.0 G oscillating field in the frequency range of 1.0–10.0 kHz under applied static magnetic fields of 1.0 (left) and 2.5 kOe (right). The solid lines are only eye-guides in (a) and (b), and best-fit curves in (c).